TransCom model simulations of CH4 and related species: Linking transport, surface flux and chemical loss with CH4 variablity in troposphere and lower stratosphere

P. K. Patra, S. Houweling, M. Krol, P. Bousquet, D. Belikov, D. Bergmann, H. Bian, P. Cameron-Smith, A. Fortems-Cheiny, M. Chipperfield, K. Corbin, A. Fraser, P. Hess, A. Ito, S. Kawa, R. Law, Z. Loh, S. Maksyutov, L. Meng, P. Palmer, R. Prinn, M. Rigby, R. Saito, C. Wilson

TransCom model simulations of CH$_4$ and related species: linking transport, surface flux and chemical loss with CH$_4$ variability in the troposphere and lower stratosphere

P. K. Patra[1], **S. Houweling**[2,3], **M. Krol**[4,3,2], **P. Bousquet**[5], **D. Belikov**[6], **D. Bergmann**[7], **H. Bian**[8], **P. Cameron-Smith**[7], **M. P. Chipperfield**[9], **K. Corbin**[10], **A. Fortems-Cheiney**[5], **A. Fraser**[11], **E. Gloor**[9], **P. Hess**[12], **A. Ito**[6,1], **S. R. Kawa**[8], **R. M. Law**[10], **Z. Loh**[10], **S. Maksyutov**[6], **L. Meng**[12,*], **P. I. Palmer**[11], **R. G. Prinn**[13], **M. Rigby**[13], **R. Saito**[1], **and C. Wilson**[9]

[1]Research Institute for Global Change/JAMSTEC, 3173-25 Show-machi, Yokohama, 2360001, Japan

[2]SRON Netherlands Institute for Space Research, Sorbonnelaan 2, 3584 CA Utrecht, The Netherlands

[3]Institute for Marine and Atmospheric Research Utrecht (IMAU), Princetonplein 5, 3584 CC Utrecht, The Netherlands

[4]Wageningen University and Research Centre, Droevendaalsesteeg 4, 6708 PB Wageningen, The Netherlands

[5]Universite de Versailles Saint Quentin en Yvelines (UVSQ), GIF sur YVETTE, France

[6]Center for Global Environmental Research, National Institute for Environmental Studies, 16-2 Onogawa, Tsukuba, Ibaraki, 305-8506, Japan

[7]Atmospheric, Earth, and Energy Division, Lawrence Livermore National Laboratory, 7000 East Avenue, Livermore, CA 94550, USA

[8]Goddard Earth Sciences and Technology Center, NASA Goddard Space Flight Center, Code 613.3, Greenbelt, MD 20771, USA

[9]Institute for Climate and Atmospheric Science, School of Earth and Environment, University of Leeds, Leeds, LS2 9JT, UK

[10]Centre for Australian Weather and Climate Research, CSIRO Marine and Atmospheric Research, 107–121 Station St., Aspendale, VIC 3195, Australia

[11]School of Geosciences, University of Edinburgh, King's Buildings, West Mains Road, Edinburgh, EH9 3JN, UK

[12]Cornell University, 2140 Snee Hall, Ithaca, NY 14850, USA

[13]Center for Global Change Science, Building 54, Massachusetts Institute of Technology, Cambridge, MA, 02139, USA

[*]now at Department of Geography and Environmental Studies Program, Western Michigan University, Kalamazoo, MI 49008, USA

Correspondence to: P. K. Patra (prabir@jamstec.go.jp)

Abstract. A chemistry-transport model (CTM) intercomparison experiment (TransCom-CH_4) has been designed to investigate the roles of surface emissions, transport and chemical loss in simulating the global methane distribution. Model simulations were conducted using twelve models and four model variants and results were archived for the period of 1990–2007. All but one model transports were driven by reanalysis products from 3 different meteorological agencies. The transport and removal of CH_4 in six different emission scenarios were simulated, with net global emissions of 513 ± 9 and $514 \pm 14\,Tg\,CH_4\,yr^{-1}$ for the 1990s and 2000s, respectively. Additionally, sulfur hexafluoride (SF_6) was simulated to check the interhemispheric transport, radon (^{222}Rn) to check the subgrid scale transport, and methyl chloroform (CH_3CCl_3) to check the chemical removal by the tropospheric hydroxyl radical (OH). The results are compared to monthly or annual mean time series of CH_4, SF_6 and CH_3CCl_3 measurements from 8 selected background sites, and to satellite observations of CH_4 in the upper troposphere and stratosphere. Most models adequately capture the vertical gradients in the stratosphere, the average long-term trends, seasonal cycles, interannual variations (IAVs) and interhemispheric (IH) gradients at the surface sites for SF_6, CH_3CCl_3 and CH_4. The vertical gradients of all tracers between the surface and the upper troposphere are consistent within the models, revealing vertical transport differences between models. An average IH exchange time of $1.39 \pm 0.18\,yr$ is derived from SF_6 time series. Rapid increase in SF_6 emissions in the tropical northern land has lead to an estimation of faster exchange time by about 11 % in the 2000s compared to the 1990s. Using six sets of emission scenarios, we show that the decadal average CH_4 growth rate likely reached equilibrium in the early 2000s due to the flattening of anthropogenic emission growth since the late 1990s. Up to 60 % of the IAVs in the observed CH_4 concentrations can be explained by accounting for the IAVs in emissions, from biomass burning and wetlands, as well as meteorology in the forward models. The modeled CH_4 budget is shown to depend strongly on the troposphere-stratosphere exchange rate and thus to the model's vertical grid structure and circulation in the lower stratosphere. The 15-model median CH_4 and CH_3CCl_3 atmospheric lifetimes are estimated to be 9.99 ± 0.08 and $4.61 \pm 0.13\,yr$, respectively, with little IAV due to transport and temperature.

1　Introduction

The variability of atmospheric CH_4 depends on the spatio-temporal variations of the surface fluxes, atmospheric transport, and destruction due to OH, Cl and O^1D chemistry. In recent years, measurements of CH_4 and related species are being conducted at an increasingly large number of sites at hourly or daily time intervals and with high instrumental precision (Rasmussen and Khalil, 1984; Aoki et al., 1990; Dlugokencky et al., 1998; Cunnold et al., 2002; WDCGG, 2010 for a complete list of observational programs). Satellite CH_4 observations from SCanning Imaging Absorption SpectroMeter for Atmospheric CartograpHY (SCIAMACHY), Atmospheric Infrared Sounder (AIRS), and Greenhouse Gases Observing SATellite (GOSAT) are also becoming available, albeit at a lower precision (Frankenberg et al., 2008; Xiong et al., 2008; Yoshida et al., 2011). Significant developments in understanding the CH_4 emission distributions have been achieved in the past two decades through forward modeling (e.g., Fung et al., 1991; Gupta et al., 1996; Houweling et al., 2000; Dentener et al., 2003; Wang et al., 2004; Patra et al., 2009a). Inverse model results show the ability of the models to reproduce the observed atmospheric CH_4 trends and variabilities within the uncertainty of the processes involved (Hein et al., 1997; Houweling et al., 1999; Mikaloff-Fletcher et al., 2004; Chen and Prinn, 2006; Bousquet et al., 2006; Bergamaschi et al., 2009). However, further improvements (reduction in the posterior emission uncertainty) of inverse modeling results depend on a better quantification of (the errors in) the prior emissions and sinks, and on error reductions in forward model transport. Presently, inverse estimates of global CH_4 emissions range between 500 to $600\,Tg\,yr^{-1}$, depending on the transport properties and the chemical loss parameterization in the forward models. Bottom-up estimations of Individual flux components vary by even greater percentages (e.g., Matthews and Fung, 1987; Yan et al., 2009).

The performance of atmospheric transport models has been investigated within the TransCom project since the early 1990s for the non-reactive tropospheric species, such as sulfur hexafluoride (SF_6) and carbon dioxide (CO_2) (Law et al., 1996, 2008; Denning et al., 1999). Convective parameterizations in CTMs have been tested through simulation of Radon (^{222}Rn), which has a radioactive decay half-life of 3.8 days (e.g., Jacob et al., 1997). The full chemistry model simulations of reactive species with a focus on ozone (O_3) chemistry have also been tested using multiple CTMs, where CH_4 is treated as a tracer with a prescribed concentration evolution (Stevenson et al., 2006 and references therein). Note that most, if not all, full chemistry models do not treat CH_4 in an interactive manner, because of its long lifetime. The CH_4 lifetime ranged from 6.3 to 12.5 yr due to large range of simulated OH concentrations in the participating models (Stevenson et al., 2006). A more conservative estimate of CH_4 lifetime is required for calculating the global warming potential (GWP) for CH_4 and its impact on climate change, or developing effective emission mitigation policies. According to Shindell et al. (2009) the 100-yr integrated GWP of CH_4 is sensitive to changes in oxidant-aerosol precursor emissions and to OH-feedbacks of CH_4 emissions itself. Proper understanding of the CH_4 budget is crucial for

these assessments.

The aim of the TransCom-CH$_4$ experiment is to quantify the role of transport, emission distribution and chemical loss in simulating the interhemispheric (IH) gradient, seasonal cycle, synoptic variation and diurnal cycle of CH$_4$. Only the first two, IH gradient and seasonal cycles, are discussed in this paper. The dependence of the CH$_4$ budget on model vertical transport in the stratosphere is also analysed. We setup a long simulation period (1988–2007, including two years of spin-up) for the following reasons: (1) in the 1990s and 2000s methane growth rates have fluctuated between 15 ppb yr^{-1} to -5 ppb yr^{-1} (Dlugokencky et al., 1998; Simpson et al., 2006; Rigby et al., 2008), and (2) we would like to obtain a better understanding of the role of emissions (using a set of six CH$_4$ emissions scenarios), chemical loss, and transport model characteristics, such as the stratosphere-troposphere exchange (STE) and the IH exchange time on CH$_4$ concentration variations in the troposphere. The proposed 18-yr simulation period allows a proper quantification of the removal fluxes in the troposphere and stratosphere and of the influence of transport processes on these removal rates. Since the previous TransCom intercomparison experiments spanned only a few years, the 18 yr of SF$_6$ simulation allows us to track the interannual variability (IAV) in the IH exchange time for the first time. We also discuss the dependence of CH$_4$ and CH$_3$CCl$_3$ lifetimes on the model grid structure and transport, as well as the transport and temperature as drivers of IAVs in lifetimes.

In Sect. 2, we describe the experimental protocol, followed by the key information on the participating models and analysis methodology. We focus this analysis (Sect. 3) on the comparison of model results with atmospheric observations of SF$_6$, CH$_3$CCl$_3$ and CH$_4$ at 8 surface sites and the salient differences in model properties. An attempt is also made to understand possible implications of (1) inert tracer (SF$_6$) transport or short-lived radioactive tracer (^{222}Rn) transport on the lifetimes and distributions of chemically active species (CH$_3$CCl$_3$, CH$_4$), and (2) the effect of the OH abundance, as constrained by CH$_3$CCl$_3$, on CH$_4$. Simulations of SF$_6$, ^{222}Rn, CH$_3$CCl$_3$ and six CH$_4$ emission scenarios are commonly referred to as model tracers. Scope for further analysis using the TransCom-CH$_4$ database and conclusions are given in Sects. 4 and 5, respectively.
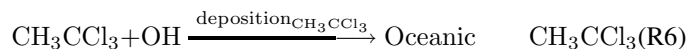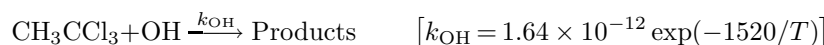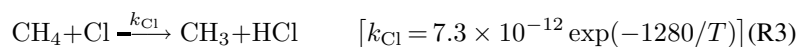
2 Models, measurements and methods

Previous TransCom experiments focused on chemically non-reactive species (SF$_6$, CO$_2$, ^{222}Rn). A CH$_4$ intercomparison requires the introduction of atmospheric chemistry. Additionally, the sources and atmospheric lifetime of CH$_4$ are distinctly different from CO$_2$, which may provide a different view on transport model differences. Detailed documentation of the requested simulation is available in the TransCom-CH$_4$ protocol (Patra et al., 2010). Chemistry-transport model simulations were requested for the period of 1 January 1990 to 31 December 2007, after a spin-up of 2-yr (1988–1989) using analyzed or atmospheric general circulation model (AGCM) meteorology or a combination of both (referred here as AGCM-nudged). A schematic diagram of TransCom-CH$_4$ model intercomparison set-up is shown in Fig. 1.

2.1 Photochemical and surface loss processes

The following chemical removal reactions for CH$_4$ (R1–R3) and CH$_3$CCl$_3$ (R4–R6) are prescribed in the forward simulations.

$$CH_4 + OH \xrightarrow{k_{OH}} CH_3 + H_2O \qquad \left[k_{OH} = 2.45 \times 10^{-12} \exp(-1775/T)\right] \text{(R1)}$$

$$CH_4 + O^1D \xrightarrow{k_{O^1D}} Products \qquad \left[k_{O^1D} = 1.5 \times 10^{-10}\right] \text{(R2)}$$

$$CH_4 + Cl \xrightarrow{k_{Cl}} CH_3 + HCl \qquad \left[k_{Cl} = 7.3 \times 10^{-12} \exp(-1280/T)\right] \text{(R3)}$$

$$CH_3CCl_3 + OH \xrightarrow{k_{OH}} Products \qquad \left[k_{OH} = 1.64 \times 10^{-12} \exp(-1520/T)\right]$$

$$CH_3CCl_3 \xrightarrow{J_{CH_3CCl_3}} Products \qquad \text{(R5)}$$

$$CH_3CCl_3 + OH \xrightarrow{deposition_{CH_3CCl_3}} Oceanic \qquad CH_3CCl_3 \text{(R6)}$$

The temperature-dependent reaction rates (k; units: cm^3 molecule^{-1} s^{-1}) are taken from the JPL synthesis of chemical kinetics (Sander et al., 2006). The monthly-mean OH fields are provided here for online calculation in the model by combining the semi-empirically calculated tropospheric (Spivakovsky et al., 2000) and 2-dimensional (2-D) model simulated stratospheric distributions. For CH$_4$ reactions with Cl and O^{1}D radicals in the stratosphere, parameterized loss rates [$k_{O^1D} \times O^1D + k_{Cl} \times Cl$] are provided, which are based on the Cambridge 2-D model (Velders, 1995).

The tropospheric OH field is reduced by 8 %, an amount that was required to optimize the agreement between the TM5 simulated and observed CH$_3$CCl$_3$ decline since 2000 (Huijnen et al., 2010). The model simulations performed here allow us to verify whether observations of CH$_3$CCl$_3$ can also be reproduced for a longer simulation period, i.e., 1990–2007, by TM5 and a variety of other models. The supplied OH field has about equal OH abundance in the northern hemisphere (NH) and the southern hemisphere (SH) (Spivakovsky et al., 2000). Since the NH/SH OH-ratio in full chemistry model simulations varies between 1.1 and 1.5 (Krol et al., unpublished data, 2008, based on the model intercomparison described in Shindell et al., 2006) we encouraged modelers to submit another set of simulations using their preferred OH field, e.g. obtained by a full chemistry version of their model.

For CH$_3$CCl$_3$ (MCF), the photolysis rates J due to solar UV radiation are provided from an Atmospheric general circulation model-based CTM (ACTM; Patra et al., 2009a) and

interpolated on each model's grid. Because the resolution in the stratosphere varies widely between models, it is necessary to scale the stratospheric loss of MCF to a common value. This value is calculated by mass-weighted averaging:

$$J_{\mathrm{av,CH_3CCl_3}} = \frac{\sum\limits_{i,j,k} J_{\mathrm{CH_3CCl_3}}(i,j,k) \times M(i,j,k)}{\sum\limits_{i,j,k} M(i,j,k)} \qquad (1)$$

Here, $M(i,j,k)$ denotes the air mass in gridbox (i,j,k) from ACTM. Modelers were required to scale their interpolated J_{MCF} field to match the $J_{\mathrm{av,MCF}}$ field of the mass-weighted annual and global mean $J_{\mathrm{av,MCF}}$ value of $7.959 \times 10^{-8}\,\mathrm{s}^{-1}$. Similarly, the annual and global mean rate constant for CH$_4$ oxidation due to stratospheric Cl and O^{1}D combined is rescaled to $2.069 \times 10^{-10}\,\mathrm{s}^{-1}$.

The monthly deposition velocities (deposition$_{\mathrm{CH_3CCl_3}}$; units: m s^{-1}) of CH$_3$CCl$_3$ to ocean surfaces are provided by Krol et al. (1998; see also Kanakidou et al., 1999). This sink should be applied in the model as:

$$\mathrm{CH_3CCl_3} = (\mathrm{CH_3CCl_3})_0 \times \exp\left(-\mathrm{deposition_{CH_3CCl_3}} \times \frac{1}{dz} \times dt\right) \qquad (2)$$

where, $dz = $ atmospheric lowest layer depth (m), $dt = $ timestep (s), and subscript 0 indicates initial concentration.

Radon decays in the atmosphere with a half-life of 3.8 days, and this decay is calculated in the model at each timestep, following

$$^{222}\mathrm{Rn} = \left(^{222}\mathrm{Rn}\right)_0 \times \exp(-dt \times 2.11 \times 10^{-6}) \qquad (3)$$

where ^{222}Rn is the radon mixing ratio at all gridpoints. This setup follows the recommendation of World Climate Research Programme (Jacob et al., 1997).

Due to the long timescales of CH$_4$ and CH$_3$CCl$_3$ oxidation and vertical transport in the stratosphere (age-of-air ~ 5 yr), several years of spin-up are required to establish realistic CH$_4$ and CH$_3$CCl$_3$ vertical profiles throughout the model atmosphere. A set of 3-D initial conditions, prepared following a 10-yr spin-up simulation by ACTM, were made available for 1 January 1988 for CH$_4$, SF$_6$ and CH$_3$CCl$_3$. CH$_4$, SF$_6$ and CH$_3$CCl$_3$ concentrations at South Pole (SPO) are 1655 ppb, 1.95 ppt and 130 ppt, respectively, for January 1988. Radon will be spun-up quickly due to its half-life of several days. Hence, its initial concentration is set to zero.

2.2 Fluxes

The typical seasonal variations of the six CH$_4$ emission scenarios are shown in Fig. 2a. Annual total emissions time series are depicted in Fig. 2b for CH$_4$, and in Fig. 2c for SF$_6$ and CH$_3$CCl$_3$. The following source and sink components of CH$_4$ were considered in the six different scenarios listed in Table 1:

1. Interannually varying anthropogenic emissions (IAV ANT), based on annual mean $1° \times 1°$ maps from the Emission Database for Global Atmospheric Research (EDGAR; version 3.2/FT) (Olivier and Berdowski, 2001). The combination of different emission categories and the inter-/extra-polation of EDGAR emission maps for the years 1990, 1995, 2000 are described elsewhere (Patra et al., 2009a).

2. Anthropogenic emissions (IAV ANT E4), based on a more advanced EDGAR database (version 4.0) (http://edgar.jrc.ec.europa.eu), where $1 \times 1°$ emission maps are available for each year until 2005. The 2005 emissions were also used for the 2006–2008 period.

3. Cyclostationary natural emissions (CYC NAT), such as those from all types of natural wetlands, domestic and large-scale biomass burning, and termites, based on the GISS inventory (Matthews and Fung, 1987; Fung et al., 1991), and emissions due to rice paddies taken from Yan et al. (2009). All these emissions are scaled as in Patra et al. (2009a). Though predominantly anthropogenic, emissions from rice cultivation are included in this category because its seasonal cycle is controlled by seasonal rainfall and temperature. The emissions due to oceanic exchange ($\sim 10\,\mathrm{Tg\,CH_4\,yr^{-1}}$) are distributed over the coastal region (Lambert and Schmidt, 1993; Houweling et al., 1999) and mud volcano emissions are based upon Etiope and Milkov (2004).

4. Wetland emissions with interannual variation (IAV WL) have been derived from the wetland emission module of the ORganizing Carbon and Hydrology in Dynamic EcosystEms (ORCHIDEE) terrestrial ecosystem model (Ringeval et al., 2010). This model uses satellite-derived area of inundation for the period of 1994–2000 (Prigent et al., 2007). The emission is scaled by a multiplication factor of 0.76 to match the wetland emission component in CYC NAT. An average seasonal cycle is used for the rest of the simulation periods (1988–1993 and 2001–2008).

5. Second set of wetland and rice emissions (IAV WLe) is obtained from the Vegetation Integrative Simulator for Trace gases (VISIT) terrestrial ecosystem model (Ito, 2010), which calculates inundated area based on analyzed rainfall, temperature (Mitchell and Jones, 2005). The rice and wetland emissions are scaled by 0.895 and 0.69, respectively, to match with CYC NAT.

6. Biomass burning emissions (IAV BB) are taken from the Global Fire Emission Database (GFED version 2), representing mainly forest and savannah burning (van der Werf et al., 2006). Since this dataset is available only after 1997, an average seasonal cycle is used for the 1988–1996 period. Unlike the wetland emissions,

global total IAV BB emissions are lower than those incorporated in CYC NAT. Thus biomass burning emissions in CYC NAT is only partially replaced by IAV BB (see Table 1). This methodology is likely to double count some of the open burning and to underestimate the emissions from closed burning.

7. Inversion-derived emissions (IAV INV) are obtained by optimizing surface fluxes to reproduce the measured CH_4 concentrations using the LMDZ model for the period of 1988–2005 (Bousquet et al., 2006). An average seasonal cycle is repeated for 2006–2008.

8. The soil sink represents a climatological average year, accounting for seasonality, derived from the LMDZ atmospheric CH_4 inversion (Bousquet et al., 2006). The global total removal amounts to 27.21 Tg CH_4 yr^{-1}.

The integrated CH_4 emissions for the different combinations of emission fields (scenario 1 to 6 in Table 1) agree within 3 Tg CH_4 over 1990–2005 (8675 Tg CH_4 for CH_4_CTL, which is 542 Tg yr^{-1} on average). Only the IAV INV scenario total emissions are slightly lower (8641 Tg CH_4).

Three other species (SF$_6$, ^{222}Radon and CH_3CCl_3) are simulated using the following fluxes:

1. Annual mean SF$_6$ emission distributions at $1 \times 1°$ are taken from EDGAR 4.0 (2009) for the period 1988–2005, and the global totals are scaled to Levin et al. (2010). The 2005 distribution is used from 2006 onwards. SF$_6$ emissions increased from 4.77 Tg yr^{-1} in 1990 to 6.79 Tg yr^{-1} in 2007.

2. Radon emissions are constructed based on the surface type in each model grid-cell; 0 poleward of $70°$, 8.23×10^{-23} mol m^{-2} s^{-1} for 60–70°, and 1.66×10^{-20} and 8.30×10^{-23} mol m^{-2} s^{-1} for land and ocean grids, respectively, within $60°$ S–$60°$ N (Jacob et al., 1997). Radon emission fields were not rescaled to match a global total source, but are expected to produce a global radon source of approximately 2.2×10^{-6} mol s^{-1}.

3. The annual mean CH_3CCl_3 emission distribution is taken from EDGAR3.2 and linearly corrected for the global totals following McCulloch and Midgley (2001) for the period 1988–1998. Emissions for 1999 to 2002 are taken as 27.5, 26.0, 17.7, and 16.1 Gg yr^{-1}, respectively. After 2002, the regional emission trends follow an exponential decay with a timescale of 5 yr (Krol et al., 2003; updated).

2.3 Participating models and output

Twelve chemistry-transport models and four of their variants (2 at higher horizontal resolution and 2 using different

OH, Cl and O(^{1}D) fields) have submitted simulation results for the period 1990–2007 (Table 2). Half of these models (ACTM, CCAM, IMPACT, LMDZ, PCTM, TM5) also participated in the previous TransCom continuous experiment, where they were tested for interhemispheric transport using SF$_6$, and synoptic and diurnal scale variability using continuous CO_2 measurements at surface sites (Law et al., 2008; Patra et al., 2008). Six other models (ACCESS, CAM, GEOS-Chem, MOZART, NIES08i, TOMCAT) participated for the first time in a TransCom experiment. The model horizontal resolution varied from $1 \times 1°$ longitude $\times$ latitude to $6 \times 4°$. In the vertical, 19 to 67 levels were employed. Salient features of each model configurations (resolutions, meteorological fields) are given in Table 2 for guidance purpose only, and do not automatically link with model performance as evaluated for various features in this study.

Concerning the wind field and other meteorology, all models, except ACCESS, used meteorological fields from weather forecast models either by interpolation (offline models) or by nudging towards horizontal winds (U, V) and temperature (online models). Most models generated output as 1-hourly averages, except LMDZ and MOZART, which provided output as 3-hourly averages.

Details of individual transport models can be found in the following references; ACCESS (Corbin and Law, 2011), ACTM and ACTM_OH (Patra et al., 2009a,b), CAM (Gent et al., 2009), CCAM (Law et al., 2006), GEOS-Chem and GEOS-Chem_DOH (Pickett-Heaps et al., 2011; Fraser et al., 2011), IMPACT and IMPACT_1×1.25 (Rotman et al., 2004), LMDZ (version 4; Hourdin et al., 2006), MOZART (version 4; Emmons et al., 2010), NIES08i (Belikov et al., 2011), PCTM (Kawa et al., 2004), TM5 and TM5_1×1 (Krol et al., 2005), TOMCAT (Chipperfield, 2006).

The TransCom-CH_4 experiment archived model simulations for 18 yrs and 9 tracers. We have sampled model output at 280 surface sites and 115 vertical profile sites (at all model levels within the troposphere) at hourly time intervals. 3-D output at 17 standard pressure levels for monthly-means for 1990–2007, and noon-time daily values for 2001–2007 are also archived.

2.4 Observational data sources and processing

Selected sites from the Advanced Global Atmospheric Gases Experiment (AGAGE; http://agage.eas.gatech.edu) and the NOAA Earth System Research Laboratory, Global Monitoring Division (http://www.esrl.noaa.gov/gmd) networks are used in this study. These sites all have simultaneous measurements of CH_4, SF$_6$, and CH_3CCl_3 covering the 1990s and 2000s (Table 4). Unfortunately, radon measurements are not available for most of these sites. Monthly or annual mean observations have been calculated from continuous (hourly averages) or flask sampling (events) measurements data available from the World Data Center for Greenhouse Gases website (WDCGG, 2010). NOAA flasks are usually sampled un-

der clean air (or baseline) conditions; this is usually onshore flow at coastal sites. The AGAGE continuous records have been flagged to remove local and regional pollution events.

The model outputs are extracted for the corresponding sites and sampling time from the hourly surface data files. For all the models, we have chosen the BRWOCN and CGOOCN sites, the nearest ocean grid to the site, to better represent baseline conditions. However, note that some models, e.g., TM5, interpolate model output to the site locations, and submit identical values at the land and ocean grids for the coastal sites. The results of HBA ($75.6°$ S, $26.5°$ W, 10 m) site are used as a replacement for the SPO site for PCTM. These selections are made as per the modeler's advice.

For CH_4, the NOAA4 calibration scale (Dlugokencky et al., 2005) agrees within 5 ppb with the AGAGE/Tohoku University calibration scale (Aoki et al., 1990). The calibration scales for CH_3CCl_3 are as per the Scripps Institution of Oceanography (SIO) 2005 (Prinn et al. 2005) for AGAGE and NOAA2003 (http://www.esrl.noaa.gov/gmd/ccl/scales/CH3CCl3_scale.html) for NOAA sites. Those for SF_6 are based on SIO 2005 (Rigby et al. 2010) and NOAA6 (http://www.esrl.noaa.gov/gmd/ccl/sf6_scale.html). The AGAGE and NOAA scales for SF_6 are in excellent agreement (NOAA–AGAGE $= 0.02 \pm 0.01$ ppt, compared to repeatability of the analytical system of 0.04 ppt) (Rigby et al., 2010). The systematic NOAA–AGAGE difference of ~ 4 ppt in 1992 reduces linearly to around 0 ppt in 2001 for the CH_3CCl_3 concentrations as determined from co-samples measurements at CGO, SMO and MHD by both the networks (Paul Krummel and Tim Arnold, personal communication, 2010).

As a check for the stratospheric CH_4 distribution simulated by the models, a climatology of CH_4 vertical profiles measured by the ACE-FTS (Atmospheric Chemistry Experiment - Fourier Transform Spectrometer) instrument onboard the SCISAT-1 satellite in the upper troposphere and stratosphere altitudes has been used (De Mazière et al., 2008). Please note that the data coverage of the ACE-FTS instrument in the tropical region is sparse. The HALOE/UARS (Halogen Occultation Experiment onboard the Upper Atmosphere Research Satellite) (Park et al., 1996) had a denser coverage and measurements of stratospheric CH_4 from this are also used for validating simulated vertical gradients in the tropical stratosphere (100–10 mb).

For this analysis, the models were sampled within 1 to 3 h of the sampling times of the measurements. Time series were constructed of monthly or annual mean samples for verification of model simulated seasonal cycles and interannual variability, respectively. The Pearson's moment correlation (Press et al., 1986) analysis is performed to evaluate the agreements between the simulated and observed time series for seasonal cycles and interannual variations at the 8 selected sites.

2.5 Calculation of IH gradients, IH exchange time, and atmospheric lifetimes

The IH exchange time (τ_{ex}) is estimated from the SF_6 annual mean concentration time series and the ratio of emission in the NH (E_n) and SH (E_s) using (Patra et al., 2009b and references therein):

$$\tau_{ex} = \left[\Delta c_{n-s} \left(\frac{E_n}{E_s} + 1 \right) \right] / \left[\frac{E_n}{E_s} \frac{dc_s}{dt} - \frac{dc_n}{dt} \right] \qquad (4)$$

c_s and c_n are the average concentrations of SH and NH sites, and Δc_{n-s} is IH concentration gradient. We used two sites in the NH (BRW, MLO) and SH (CGO, SPO) to estimate the hemispheric average concentrations c_n and c_s, respectively, at yearly time intervals (dt). Because SF_6 measurements at ALT are not available after 2005, BRW is chosen for this analysis. The values $c_n - c_s$ are shown as IH gradients of each species. We have tested that the calculated τ_{ex} does not depend strongly on the $\frac{E_n}{E_s}$ ratio.

We also estimated CH_4 and CH_3CCl_3 lifetimes (τ) using the mass balance equation

$$\frac{dB}{dt} = E - L = E - \frac{B}{\tau} \qquad (5)$$

B, E and L are the annual total atmospheric burden, surface emission and photochemical loss, respectively. As approximate estimates of B, average concentrations of CH_4 and CH_3CCl_3 for 8 sites are multiplied by the concentration-to-mass conversion factors of $2.845\,Tg\,CH_4\,ppb^{-1}$ and $23.689\,Gg\,CH_3CCl_3\,ppt^{-1}$, respectively. Ideally, vertical distribution properties of each species should be accounted for with appropriate air mass factors for calculating B. However, we note that the average lifetimes over the period of 2000–2007 calculated using ACTM simulated gridded loss rates agree within 0.01 yr for CH_3CCl_3 with the lifetimes calculated using Eqn. (5) suggesting that the simplification is acceptable.

3 Results and discussions

3.1 Zonal mean concentrations

Figure 3 compares the latitude-pressure variations of the zonal mean CH_4_CTL scenario in the troposphere and lower stratosphere to representative ACE-FTS measurements (please refer to Figs. S1–S17 for individual model comparison plots of ^{222}Rn, SF_6 and CH_4 along the $70°$ E and $180°$ E longitudes, and zonal mean CH_3CCl_3 distributions corresponding to the years 1994 and 2005). Generally, all models exhibit similar large-scale features, equator-pole latitudinal gradients, and vertical gradients in the lower stratosphere. Most significantly different, however, is the transition

between the troposphere and stratosphere and the heights at which the vertical gradients maximize in the models (the green-to-blue shaded regions). The ACCESS/GEOS-Chem/NIES-08i and CAM/MOZART/CCAM models show the maximum and minimum decrease rates of CH_4 with increasing height, respectively, in the height range of 100–50 mb. CAM, CCAM and MOZART models have only few vertical layers above 100 mb and use the same reanalysis wind fields from NCEP, and the NIES model employs isentropic coordinate system in the stratosphere. The formulation of models is known to affect the simulation of tracer gradients in the upper troposphere/lower stratosphere region. `A version of the TOMCAT/SLIMCAT model, which uses isentropic coordinates in the stratosphere, produces stronger tracer gradients and a more realistic Brewer Dobson circulation than the p-coordinate version used here (e.g., Hossaini et al., 2010 and references therein).` The "tropical pipe" (Plumb, 1996) along the upward transport branch of the Brewer-Dobson circulation appears more "leaky" in the models than in the limb-viewing remote sensing observations by HALOE and ACE-FTS. As a result, the simulated concentration isopleths appear flatter compared to the observations with increasing latitudes in both hemispheres. The CH_4 meridional gradients between tropics (Eq–10° N) and northern extratropics (20° N–30° N) are calculated to be 140 ± 72 ppb for the models and 225 ppb for HALOE in the height range of 70–30 mb.

In the troposphere, vertical transport of the NH emission varies between the models, most prominently in the tropical region, where deep cumulus convection is prevalent. Table 3 shows mean vertical gradients and between model variabilities in three broad latitude ranges. Model to model differences are much less distinct at the mid and high latitudes than in the tropics for SF_6, CH_4 and CH_3CCl_3. However, two main categories of models can be identified based on the density of CH_4 isopleths in the height range between 350 and 200 mb. The position and concentration gradient across the tropopause differs considerably among models. These model features are also present in the SF_6 simulations suggesting the predominant role of transport in the simulation of the CH_4 vertical distributions. The penetrative mass flux due to deep cumulus convection in tropical latitudes is strongest in ACTM and GEOS-Chem (low ^{222}Rn concentration difference of $\sim 5.63 \times 10^{-21}$ between 850 and 200 mb), and relatively weaker in NIES08i, PCTM and TOMCAT (high ^{222}Rn concentration difference $> 12 \times 10^{-21}$). This is clearer from the simulated ^{222}Rn distributions over the South Asian monsoon region at 70° E during boreal summer (Figs. S2 and S4). It has been shown in Patra et al. (2009b), based on ACTM simulations with and without cumulus parameterization, that deep cumulus convective transport is the main cause for rapid vertical transport of tracers to

the upper troposphere (seen as higher ^{222}Rn concentrations compared to the lower troposphere). `Feng et al (2011) showed that the online convection scheme used in the TOMCAT runs for this study underestimated the ECMWF archived convective mass fluxes especially in terms of the altitude extent of deep convection in the tropics.` The higher horizontal resolution versions of both IMPACT and TM5 resulted in higher ^{222}Rn concentrations in the middle-upper troposphere (i.e., smaller difference between 850 mb and 400/200 mb) compared to their respective lower resolution simulations. This is suggesting that some convective processes are being resolved in higher resolution models that are not present in the lower resolution models.

3.2 Model-observation comparison of CH_4, SF_6 and CH_3CCl_3
Annual means: 1990–2007

Figure 4 shows the time series of annual mean concentration differences between simulated and observed CH_4, SF_6 and CH_3CCl_3 at two selected sites (MLO and CGO). First SF_6 is considered, which has no chemical loss (middle row). Typical model behaviour is similar at all 8 sites (not shown). For most models, the simulated concentrations divert from the measurements by 0.2 ppt in 1995, after which differences remain at that level. The offsets between models can be explained by initial values assumed by each models. Only ACCESS shows increasing differences in time until 2006. The ACTM_OH case, which uses EDGAR4.0 emissions without scaling between 1988–2005, and 2005 emission for 2006 and 2007 and produces a slower increase in the model concentration compared to observations after 2000. This suggests that the global total emissions estimated by Levin et al. (2010) and later confirmed by Rigby et al. (2010) are adequate also for independent state-of-the-art transport models.

The CH_3CCl_3 simulations are of an intermediate level of uncertainty, as this species is emitted to the atmosphere by a relatively well quantified industrial use as a solvent. However, uncertainties remain for its loss by reaction with OH in the troposphere, photolysis in the stratosphere and the rate of STE. Until 1990, CH_3CCl_3 emissions were increasing, followed by near-exponential decrease due to stringent restriction of its production/use by the Montreal Protocol (WMO/SAOD, 2003). The lifetimes of CH_3CCl_3 due to photochemical removal is much longer in the stratosphere (~ 28.6 yr) than in the troposphere (~ 5.8 yr) (estimates from ACTM simulated loss rates at model grids; similar estimates of lifetimes using TM5 are 28.6 and 5.8 yr, respectively). Thus the troposphere to stratosphere transport plays a minor role in the global total budget of CH_3CCl_3 after the late 1990s, because the concentration gradients across the tropopause reduced to less than 10 ppt (ref. Table 3). Although these lifetimes in the stratosphere and troposphere

are within the range of independent estimates, 38^{+15}_{-11} and $6^{+0.5}_{-0.4}$ yr, respectively (Prinn et al., 2005), both the mean values are lower for ACTM. Despite the fact that the models were initialized using the same concentration at 1 January 1988, significant differences in the simulated concentrations are found already for 1990, after two years of simulation. The established model-measurement differences in 1990 persist until the end of the simulations (LMDZ CH_3CCl_3 being the only outlier) even though the CH_3CCl_3 concentrations become very small towards 2007. Given the CH_3CCl_3 lifetime of less than 5 yr, these differences are caused by differences in transport and removal rather than the initialization.

CH_4 is the most complicated species considered in the TransCom-CH_4 experiment, because the CH_4 surface emissions and effect of STE are less certain than for CH_3CCl_3. Generally, the models that simulate lower CH_3CCl_3 concentrations compared to the multi-model mean, also yield lower CH_4 concentrations (such as MOZART, CCAM). For example, the high and low-resolution TM5 simulations show the highest concentrations of both CH_4 and CH_3CCl_3 at MLO. However, it is interesting to note that GEOS-Chem (with TransCom OH) calculates the lowest CH_4 concentrations among all models, while the simulated CH_3CCl_3 levels are not distinctly different. LMDZ is among the models that most strongly underestimate the observed level of CH_3CCl_3, whereas the opposite is true for CH_4 (Fig. 4). These contrasting behaviors among models for various CH_4 and CH_3CCl_3 simulations clearly suggest that CH_4 loss due to the reaction with OH in the troposphere is not the only control on the CH_4 budget differences between models and that other factors such as transport differences also play a role (details in sections 3.3 and 3.4).

3.2.1 Seasonal cycles

Figure 5 shows model to measurement comparisons of the seasonal cycles of CH_4, SF_6 and CH_3CCl_3 at three selected sites (MLO, SMO and CGO) for the period 2002–2003. These sites have been selected because they are at large distances from the continental emissions for each of these species. To highlight differences in seasonality, approximate linear trends and offsets corresponding to the period 2002–2003 have been subtracted from the monthly-mean values. All models capture the salient features in the seasonal cycles at very high statistical significance (ref. Table 4 for correlation coefficients at 8 sites), except for SF_6 at MLO, where the measurements show unusual fluctuations and a large data gap during 2002. Even for the years with dense data coverage (2005–2006), low average correlation coefficients (r) of 0.3 for the SF_6 seasonal cycles at MLO are obtained due to a very small seasonal cycle of less than 0.04 ppt. In contrast, the clear seasonalities (amplitude > 0.04 ppt) at ALT, MHD, SMO, CGO and SPO are well reproduced by the models ($r > 0.4$; significant at $P = 0.05$ in two tailed Student's t-test for 24 data points). The fact that the models are able

to reproduce the observed seasonal cycles indicates that even though the signals are weak, they nevertheless provide useful information for model validation. All models reproduce the CH_3CCl_3 seasonal cycle fairly well at all 8 sites, both in phase and amplitude ($r > 0.8$).

For CH_4, the influence of the surface flux on the simulated seasonal cycles can be studied using the 6 different CH_4 scenarios. The corresponding correlation coefficients, listed in Table 4, suggest that the CH_4 seasonal cycle depends strongly on the implemented wetland and biomass burning fluxes. The CH_4_INV simulations consistently produce higher correlation coefficients at all the NH sites (ALT, BRW, MHD, MLO and RPB), which was expected because the atmospheric-CH_4 inversion used data from these sites for flux optimization. CH_4_EXTRA results are next best in comparison with measured seasonal cycles for the NH high latitude sites. For any given tracer, the correlation coefficients are highest at remote SH sites, CGO and SPO, compared to all other sites. The use of ACTM_OH and GEOS-Chem_DOH or the higher horizontal resolution versions of IMPACT_1×1.25 and TM5_1×1 do not always improve the agreement between model and observations compared to the default implementation. These results suggest a need for improving our understanding of the CH_4 flux seasonality in the Northern Hemisphere land regions, noting that the OH loss is realistically represented as seen in the simulated CH_3CCl_3 seasonal cycles. Because ACCESS (blue line) was not run with analyzed winds and temperature, the simulated seasonal cycles are not as good as other models for CH_4 and SF_6 highlighting the role of meteorology in simulating tracer concentrations. The role of meteorology is less pronounced for CH_3CCl_3 because the emissions are weak in the 2000s. A more detailed analysis of seasonality at a larger number of sites will be conducted in a future study.

3.2.2 Interannual variability (IAV)

We calculated growth rates for all tracers as the difference between annual mean concentrations for two adjacent years. The growth rate at January 2000 is shown as the difference between 1999 and 2000 mean concentrations. The simulated and observed SF_6 growth rates (not shown) decreased from ~ 0.25 ppt yr^{-1} in 1997 to ~ 0.2 ppt yr^{-1} in 2000. Afterwards, the growth rate steadily increased to ~ 0.25 ppt yr^{-1} in 2006 (please refer to Table 4 for correlation coefficients; $r \sim 0.7$ for 5 sites). The length of time series considered for the correlation calculation of the IAVs is 1990–2007 for CH_4 (except for CH_4_WL_BB, which has 7 yr of IAV, 1994–2000) and CH_3CCl_3, and 1996–2007 for SF_6 (the period when observations are available). The correlation coefficients greater than 0.44 and 0.53 are statistically significant at $P = 0.05$ for 18 and 12 data points, respectively. Average CH_3CCl_3 growth rates (not shown) hovered around 0 to 5, -12 to -17 and ~ -2.5 ppt yr^{-1} during 1991, 1997 and 2007, respectively, with gradual changes in between. These tempo-

ral variations are well simulated by all models ($r > 0.9$). Because both SF_6 and CH_3CCl_3 emissions are of purely anthropogenic origin, their production, consumption and release to the atmosphere vary relatively smoothly in comparison to the natural components of CH_4 emissions.

Figure 6 shows the model-observation comparison of the IAV in CH_4 growth rates for three broad latitude regions: the NH, tropics and SH corresponding to the CTL and EXTRA emissions (refer to Figs. S20 and S21 for others). Averaged observed CH_4 growth rates for the 1990s are 5.25, 5.06 and 7.01 ppb yr^{-1} in the NH, tropics and SH, respectively. Almost no increase in concentration is observed for the 2000s (except for 2007). Additionally, it can be seen that the IAVs in the growth rate are higher at the NH sites compared to the tropical and SH sites. Figure 6 shows that although the CH_4_CTL simulations capture the observed reduction in the decadal average growth rates, the IAV is not well reproduced. Most prominent is the 1997/1998 El Niño event (Langenfelds et al., 2002). During this event the observations show an increase, while the simulations show a decrease in the growth rate. Interestingly, the CH_4_CTL emission and OH concentration (both without IAV) cannot explain this model behavior, which is therefore attributed to the increased $CH_4 + OH$ reaction rate as modified by CH_4 transport and temperature in the model. This, in turn, is caused by the El Niño induced higher air temperatures (Reaction R1), resulting in faster removal of CH_4 from the troposphere and thus a decrease in the growth rate. Indeed, the 1998 CH_4_CTL lifetime (9.82 yr) is estimated to be the shortest among all simulation years.

As seen from Table 4, inclusion of biomass burning emission IAV (CH_4_BB) improves the IAV model-observation agreement at all sites compared to CH_4_CTL. However, when wetland emissions are included (CH_4_WL_BB), the correlations tend to deteriorate. Compared to CH_4_BB, only CH_4_EXTRA produces better model-observation agreement for growth rates (Fig. 6, right panels). The wetland CH_4 emission simulated by the VISIT ecosystem model included in CH_4_EXTRA displays a large positive anomaly on top of the emissions from biomass burning during 1997/1998. Combined, these emissions compensate for the extra CH_4 loss due to higher air temperatures. As a consequence, these emissions result in an excellent agreement with the growth rates observed at the SH and NH sites (except that the simulated tropical signal is a bit too strong in 1998). The IAV of the multi-model average CH_4 growth rate at BRW did not correlate significantly with the observed IAV because this site is located close to the Alaskan wetland region, and the site representation error is large for the coastal sites in coarse resolution global models (Patra et al., 2008).

The decreasing growth rate in the 1990s, near zero growth rates in early 2000s and the reappearance of positive CH_4 growth in the late 2000s have drawn considerable interests for developing emission inventories. For example, Lamarque et al. (2010) suggested a decrease of CH_4 emissions by about 40 Tg CH_4 from 1990 to 2000 for simulating the zero CH_4 growth rate in the early 2000s using the CAM-Chem model. Their estimate is largely inconsistent with our results, which is suggesting that a steady state is achieved between CH_4 chemical destruction and emissions during the early 2000s (Dlugokencky et al., 2003). The EDGAR4.0 anthropogenic CH_4 emission increase of ~ 4 Tg CH_4 yr^{-1} during 2001–2007, synchronized with the Chinese economic growth, produces inconsistencies between observed and simulated growth rates during 2003–2007 (thus the lowest correlation coefficients for the growth rate IAVs in Table 4; see also Fig. S20). This indicates that forward simulations using multiple forward transport models are useful for the verification of emission inventories.

3.3 Interhemispheric gradients and exchange times

Figure 7 shows the concentration gradients between two NH sites and two SH sites obtained using annual mean observed and modeled time series. All models except for the TM5s, simulate the observed SF_6 IH gradient within the measurement accuracy of ± 0.057 ppt ($\sqrt{2} \times$ measurement precision). These gradients translate to an average IH exchange time (τ_{ex}) of 1.39 ± 0.18 yr (for all models and years), which is an indication of close model-model agreement (Fig. 8). This model-model spread is much smaller compared to the model pool of the 1990s (Denning et al., 1999), which gave τ_{ex} range of 0.8–2.0 yr. In this intercomparison, the τ_{ex} range between models is 0.62 ± 0.06 yr compared to 1.2 yr in the TransCom experiment during the 1990s. The average τ_{ex} of 1.39 yr is in excellent agreement with the estimates of 1.3 yr (Geller et al., 1997) and 1.5 yr (Levin and Hesshaimer, 1996), derived using measured SF_6 time series. The underestimation by ACTM_OH version is due to smaller SF_6 emissions (note: this version used EDGAR4.0 without scaling), highlighting the role of the emission strength in the forward model simulations.

A tendency towards faster IH exchange time is seen for both the observations and the simulations (a decrease in exchange time by about 0.2 and 0.15 yr, respectively) between 1996–1999 and 2004–2007. This decrease in τ_{ex} can have large implications for estimating fluxes of long-lived species by inverse modelling, especially for the trends in hemispheric emissions and sinks ratio. We further probe the decrease in τ_{ex} by simulating SF_6 concentrations using three emission scenarios; 1. same as in TransCom–CH_4 protocol (EDGAR4.0/Levin), 2. the EDGAR4.0 emission distribution corresponding to 2000, but global totals scaled to Levin et al. (2010) (EDGAR_Y2000/Levin), and 3. constant emissions from EDGAR4.0 for the year

2000. Because this set of simulations
are designed in October 2011, following
the suggestions by Ingeborg Levin (pers.
comm., Rome), one model (ACTM) is used
for this experiment. Fig. 9a shows the
trends in SF_6 emissions within three
broad latitude bands. The emissions
in the NH mid-high latitudes (circles)
remained fairly constant (within 14%),
while the emissions from the NH tropical
latitudes increased by more than 100%
during 1998 to 2007. The estimated
τ_{ex} using three emission scenarios are
shown in Fig. 9b. These results clearly
suggest that the strong decrease rate
in τ_{ex} is valid only in Case 1 (0.19 yr
per decade), and the decrease rate
become an order of manitude smaller
as well as statistically insignificant
(r=-0.32, N=12) when SF_6 emissions were
kept constant (Case 3). The decrease
in τ_{ex} remained significant for Case
2, suggesting that difference in net
emissions in NH and SH effect the
estimation of τ_{ex} using Eqn. 4. In
Case 2, the $\frac{E_n}{E_s}$ ratio was fixed at 36.9
corresponding to the year 2000, but
total SF_6 emission in the NH increased
faster rates. Our results also suggest
that more number of boxes should be
introduced for accounting the time
evolution of regional changes in SF_6
emissions for calculating τ_{ex}.

All three long-lived species show a similar relationship for the IH gradient: the model that produces a larger (smaller) SF_6 IH gradient generally also produces a larger (smaller) IH gradients for CH_3CCl_3 and CH_4 in comparison with the observations (Fig. 10). The intriguing exception is MOZART, which exhibits an excellent match for SF_6 IH gradient, but produces one of the largest CH_4 IH gradients (127 ppb compared to an observed value of 101 ppb) and one of the smallest CH_3CCl_3 gradients (0.13 ppt) during 2003–2007. Similar contrasting behaviour is also seen for several other models at lesser distinction, e.g., GEOS-Chem_DOH, NIES-08i lie above the fitted line for CH_4, but lie below the fitted line for CH_3CCl_3. The CH_4 IH gradients are best reproduced using the CH4_INV emissions: deviations are within 5 ppb for 7 models (Fig. 10). Taking into account the IH gradient of all three species, TM5/CCAM, ACTM/IMPACT_1×1/PCTM and LMDZ/NIES-08 showed systematically higher, similar and lower IH gradients, respectively, compared to the observations.

Two models submitted simulations using
different OH, which can be used for
understanding the role of IH gradients
in OH on the simulated CH_4 and CH_3CCl_3
IH gradients. The NH/SH ratio of
hemispheric total tropospheric OH are
(1) 1.32 for ACTM_OH and (2) 1.11 for
GEOS-Chem_DOH, while that (Spivakovsky
et al., 2000) used in ACTM is 0.99. The
observed CH_4 IH gradient is 100.97 ppb,
while the simulated gradients from ACTM
and ACTM_OH are 99.99 and 87.45 ppb,
respectively. In order to simulate the
observed CH_4 IH gradient, the NH/SH
OH ratio for ACTM would need to be
0.96 [= 0.99 + (1.32 − 0.99) × $\frac{(99.99-100.97)}{(99.99-87.45)}$].
This is close to the NH/SH OH ratio
derived by Spivakovsky et al. (2000).
Note also that the ACTM simulations of
both CH_3CCl_3 and SF_6 agree very well
with the observations. Similarly, to
simulate the observed CH_4 IH gradient,
the NH/SH OH ratio for GEOS-Chem
model should be 1.15 [= 0.99 + (1.32 −
0.99) × $\frac{(107.53-100.97)}{(107.53-102.65)}$]. Both GEOS-Chem
model versions simulate greater IH
gradients also for CH_3CCl_3, a species
that has been used for benchmarking
tropospheric OH concentrations and
distributions. However, the GEOS-Chem
simulated SF_6 IH gradient agrees very
well with the observed and ACTM results.
Given the small amount of alternative
OH distributions in models and the
remaining uncertainties in CH_4 and
CH_3CCl_3 emissions, our best judgement
at the moment is that we cannot falsify
the NH/SH gradient (0.99) derived by
Spivakovsky et al. (2000).

3.4 Photochemical removal of CH_4 and the role of transport

The calculated photochemical loss of CH_4 varies between 490 and 509 Tg CH_4 yr^{-1} during the first eight years (1992–1999), and between 497 and 513 Tg CH_4 yr^{-1} during the last eight years (2000–2007) of the simulation. Figure 11a suggests that the eight-years averaged growth rates at the surface sites for the different models are, as expected, inversely proportional to the calculated photochemical destruction. However, this relationship appears loose, particularly for 2000–2007, when the models approach steady state (correlation coefficient, $r = -0.42$ for all models, but increase to -0.82 and -0.61 for 1990s and 2000s, respectively, by excluding NIES-08i). Possible explanations are investigated in Fig. 11b, using the vertical gradients in the equatorial lower stratosphere (CH_4 at 100 mb – CH_4 at 10 mb; zonal average for 5° S–5° N latitudes). Models showing greater gradients

have slower Brewer-Dobson circulation, and thus stronger trapping of CH$_4$ in the troposphere, resulting in faster CH$_4$ destruction and smaller growth rate because CH$_4$ lifetime in the troposphere is an order of magnitude shorter than that in the stratosphere. Although these relationships are again quite loose during the 1990s, as the models attain their steady state, statistically significant correlations ($r = -0.69$) are found for the period of 2000–2007 between the CH$_4$ growth rates and vertical gradients in the lower stratosphere. While the growth rates decrease from the 1992–1999 period to the 2000–2007 period in all models, the modeled gradients remain remarkably constant. Based on this analysis we suggest that the simulated concentration growth rates at the surface sites are linked to the troposphere to stratosphere transport rate of CH$_4$.

Figure 12 shows the temporal variability in the estimated lifetimes (Eqn. 5) for CH$_4$_CTL and CH$_3$CCl$_3$ (ref. Table 2 for time-averaged model specific lifetimes). The median CH$_4$ lifetime due to atmospheric loss processes (Reactions R1–R3) is 9.99 ± 0.08 (1σ for interannual variability) years and ranges from 9.50 ± 0.10 and 10.27 ± 0.14 yr for the different models. Here it should be remembered that all, but ACTM_OH and GEOS-Chem_DOH, models used the same OH distribution. The median CH$_4$ lifetime for 16 models or model variants agrees well with the lifetime (10.0 ± 0.17) estimated from the measured mean concentrations at 8-sites (Eqn. 5). This is because a close balance is achieved between the modeled atmospheric loss and net surface emissions (513 ± 9 and 514 ± 14 Tg CH$_4$ yr^{-1} for the 1990s and 2000s, respectively). The median CH$_3$CCl$_3$ lifetime due to all loss processes (Reactions R4–R6) is estimated to be 4.61 ± 0.13, 4.59 ± 0.18 and 4.62 ± 0.02 yr during the 1992–2007, 1992–1999 and 2000–2007, respectively. TM5 simulates a lifetime of 4.87 ± 0.03 yr, which is close to the estimates using the measured CH$_3$CCl$_3$ concentrations of 4.9 ± 0.3 yr (Prinn et al., 2005), 5.0 yr (WMO/SAOD, 2003) or 4.94 ± 0.15 yr (this study based on 8 sites). All other models calculated a shorter lifetime, by an average value of 0.3 yr. CAM, CCAM, LMDZ and MOZART calculate lifetimes of 4 yr or shorter. The interannual variation in the estimated CH$_3$CCl$_3$ lifetimes during the 1990s is an order of magnitude higher than that in the 2000s. We find up to 5 % variability in the modeled CH$_3$CCl$_3$ lifetimes during 1992–1999, a period with substantial emissions. During 2000–2007, when the emissions of CH$_3$CCl$_3$ dropped significantly, less than 0.4 % variability is simulated. This implies that inversions to estimate OH from CH$_3$CCl$_3$ observations are less uncertain since 2000, a finding in good agreement with Montzka et al. (2011).

4 Further work and data accessibility

For this analysis we used results of chemical tracer simulations at only 8 selected sites with measurements of atmo-

spheric CH$_4$, SF$_6$ and CH$_3$CCl$_3$, which is a very small subset of the 280 surface sites for which output is available. In addition, vertical profiles of chemical tracers and several meteorological parameters have been archived at 115 sites. More analyses on the basis of the TransCom-CH$_4$ simulations are planned focusing on (1) CH$_4$ vertical profiles measured using aircraft, (2) analysis of vertical column averaged CH$_4$ concentrations using TCCON observations, (3) using increase, decrease and exponential decay of CH$_3$CCl$_3$ for optimizing tropospheric OH abundance. We also welcome use of this data set by the measurement community. In an effort towards ease of access, time series at a subset of surface sites are archived at JAMSTEC (http://ebcrpa.jamstec.go.jp/dav/prabir/transcom-ch4/sites_data/). Information on how to access the full dataset is available in the experimental protocol, archived on this website (http://transcom.project.asu.edu/T4_methane.php).

In addition to the site-specific data, gridded output at monthly intervals at the model horizontal resolution at standard pressure levels are archived for the period 1990–2007. Afternoon averages (12:00–15:00 LT – Local Time) at daily intervals are also archived for the period 2001–2007. We believe these sets of model output, their extension to recent years, will be useful for comparing the model simulations with satellite observations (SCIAMACHY, AIRS, GOSAT) and aircraft observations (e.g., HIPPO – HIAPER Pole-to-Pole Observations of carbon cycle and greenhouse gases study, Wofsy et al., 2011).

5 Summary and conclusions

We analyzed concentration time series of CH$_4$, CH$_3$CCl$_3$, SF$_6$ and ^{222}Rn simulated by 16 chemistry-transport models as part of the TransCom-CH$_4$ intercomparison experiment. We focused the analysis on the model-to-model differences in:

1. The vertical redistribution of tracers, based on ^{222}Rn simulations and comparisons to CH$_4$ satellite observations in the upper troposphere and lower stratosphere.

2. Large-scale interhemispheric (IH) transport, by comparing modeled and observed IH gradients of SF$_6$, CH$_4$ and CH$_3$CCl$_3$.

3. Simulated seasonal cycles, by comparing to observed seasonal cycles at remote background stations.

4. Inter-annual variations in the simulated CH$_4$ growth rate, by focusing on the results of six different CH$_4$ emission time-lines.

5. The role of removal by OH on the simulated CH$_4$ and CH$_3$CCl$_3$ concentrations.

The main conclusions can be summarized as follows:

i. Although the simulated zonal mean ^{222}Rn concentrations agree between models, significant differences are observed in regions of deep cumulus convection, e.g., the south Asian summer monsoon domain. Unfortunately, observational evidence to check the model behavior is lacking. Models also differ in the simulated height of large troposphere-stratosphere concentration gradients of CH_4. Compared to CH_4 satellite observations in the upper troposphere, most models appear to be too diffusive around the tropical tropopause.

ii. The IH exchange time, calculated from the simulated SF_6 distributions, ranges from 1.79 to 1.17 yr (average over 1996–2007) for the different models. The model-average value of 1.39 yr is in close agreement with earlier studies and observational evidence. Models that show faster IH exchange for SF_6, also exhibit faster exchange (smaller IH gradients) for CH_4 and CH_3CCl_3. This multi-tracer evidence provides clear directions for the improvement of specific models. Both the exchange time calculated from the models and the time calculated from the observations suggest an acceleration of the IH exchange in the 2000s compared to the 1990s.

iii. All models reproduce the observed seasonal cycles of CH_4 and CH_3CCl_3 at background sites very well. The simulated CH_4 seasonal cycles depend on the destruction by reaction with OH, concealing the seasonality of the underlying emissions. The simulated seasonal cycles of CH_4 are influenced by the photochemical destruction by OH: without destruction, the simulated seasonal cycles would more strongly reflect the seasonal cycles present in the emission scenarios. Two of the six simulated CH_4 scenarios (CH_4_INV and CH_4_EXTRA) show a higher correlation with the observed seasonal cycle.

iv. A set of six CH_4 flux representations was used to investigate the role of specific processes in reproducing the observed interannual variations in the CH_4 growth rate. The control emission case (CH_4_CTL) without a significant increase in anthropogenic emissions and no interannual variability in natural emissions for the period 1990–2007 reproduces the declining growth rate in the 1990s, followed by the stabilization in the 2000s. Inclusion of interannual variation in emissions from the wetland and forest fires (CH_4_EXTRA) most successfully simulates the observed interannual variations in CH_4. It was also suggested that the higher tropospheric temperatures during the 1997/1998 El Niño resulted in larger CH_4 destruction, whereas the observations clearly show a rise in CH_4 concentration. To match the observations, either enhanced emissions are required (as in CH_4_EXTRA), or less than average OH should have been present in this period.

v. The simulation of CH_3CCl_3 is used to check the consistency of the employed OH abundance and distribution. Two models used an alternative OH field next to the prescribed field. Generally, models that simulate a low abundance of CH_3CCl_3 also simulate a low abundance of CH_4. However, there are exceptions, which indicates that CH_4 loss due to OH in the troposphere is not the only cause of the modeled CH_4 differences. Thus, horizontal and vertical transport differences may also be important.

vi. Further analysis reveals that the simulated CH_4 growth rate shows (weak) correlations with the modeled vertical gradient in the equatorial lower stratosphere. This suggests that differences in vertical mixing of the emissions and in stratosphere-troposphere exchange are the main causes of the model-to-model differences. Next to the interhemispheric transport in models, this issue requires further analysis, e.g. based on the archived model output.

vii. Finally, the multi-model lifetime estimates for CH_4 and CH_3CCl_3 were found to be fairly constant over the simulation period with median values of 9.99 ± 0.08 and 4.61 ± 0.13 for the period 1992 to 2007. This underscores the fact that OH (assumed constant in the simulations) is the driving factor in the budgets of these gases, and that transport and temperature (affecting the reaction rate) differences play a smaller role. We find net CH_4 emissions to the atmosphere of 513 ± 9 and $514 \pm 14\,Tg\,CH_4\,yr^{-1}$ (soil sink subtracted) for the 1990s and 2000s, respectively, are consistent with the atmospheric losses accounted for due to OH, O^1D and Cl in order to simulate CH_4 concentrations and growth rates at the surface sites.

References

Aoki, S., Nakazawa, T., Murayama, S., and Kawaguchi S.: Measurements of atmospheric methane at the Japanese Antarctic Station, Syowa, Tellus B, 44, 273–281, 1992.

Bergamaschi, P., Frankenberg, C., Meirink, J. F., Krol, M., Villani, M. G., Houweling, S., Dentener, F., Dlugokencky, E. J., Miller, J. B., Gatti, L. V., Engel, A., and Levin, I.: Inverse modeling of global and regional CH_4 emissions using SCIAMACHY satellite retrievals, J. Geophys. Res., 114, D22301, http://dx.doi.org/10.1029/2009JD012287doi:10.1029/2009JD012287, 2009.

Belikov, D., Maksyutov, S., Miyasaka, T., Saeki, T., Zhuravlev, R., and Kiryushov, B.: Mass-conserving tracer transport modelling on a reduced latitude-longitude grid with NIES-TM, Geosci. Model Dev., 4, 207–222, http://dx.doi.org/10.5194/gmd-4-207-2011doi:10.5194/gmd-4-207-2011, 2011.

Bloom, S., da Silva, A., Dee, D., Bosilovich, M., Chern, J.-D., Pawson, S., Schubert, S., Sienkiewicz, M., Stajner, I., Tan, W.-W., and Wu, M.-L.: Documentation and Validation of the Goddard Earth Observing System (GEOS) Data Assimilation System – Version 4, Technical Report Series on Global Modeling and Data Assimilation 104606, NASA Goddard Space Flight Center, Maryland, 26, 2005.

Bousquet, P., Ciais, P., Miller, J. B., Dlugokencky, E. J., Hauglustaine, D. A., Prigent, C., van der Werf, G. R., Peylin, P., Brunke, E.-G., Carouge, C., Langenfelds, R. L., Lathiére, J., Papa, F., Ramonet, M., Schmidt, M., Steele, L. P., Tyler, S. C., and White, J.: Contribution of anthropogenic and natural sources to atmospheric methane variability, Nature, 443, 439–443, http://dx.doi.org/10.1038/nature05132doi:10.1038/nature05132, 2006.

Butler, J. H., Daube, B. C., Dutton, G. S., Elkins, J. W., Hall, B. D., Hurst, D. F., King, D. B., Kline, E. S., Lafleur, B. G., Lind, J., Lovitz, S., Mondeel, D. J., Montzka, S. A., Moore, F. L., Nance, J. D., Neu, J. L., Romashkin, P. A., Scheffer, A., and Snible, W. J.: Halocarbons and other atmospheric trace species, Chapter 5, in: CMDL Summary Report No. 27, 2002–2003, edited by: Thompson, T. M., NOAA/US Department of Commerce, Boulder, USA, 115–135, 2004.

Cao, M., Gregson, K., and Marshall, S.: Global methane emission from wetlands and its sensitivity to climate change, Atmos. Environ., 32, 3293–3299, http://dx.doi.org/10.1016/S1352-2310(98)00105-8doi:10.1016/S1352-2310(98)00105-8, 1998.

Chen, Y.-H. and Prinn, R. G.: Estimation of atmospheric methane emissions between 1996–2001 using a 3-D global chemical transport model, J. Geophys. Res., 111, D10307, http://dx.doi.org/10.1029/2005JD006058doi:10.1029/2005JD006058, 2006.

Chipperfield, M. P.: New version of the TOMCAT/SLIMCAT offline chemical transport model: intercomparison of stratospheric tracer experiments, Q. J. Roy. Meteorol. Soc., 132, 1179–1203, http://dx.doi.org/10.1256/qj.05.51doi:10.1256/qj.05.51, 2006.

Corbin, K. D. and Law, R. M.: Extending atmospheric CO_2 and tracer capabilities in ACCESS, CAWCR Technical Report No. 35, The Centre for Australian Weather and Climate Research, ISBN: 978-1-921826-177, Aspendale, 2011.

Cunnold, D. M., Steele, L. P., Fraser, P. J., Simmonds, P. G., Prinn, R. G., Weiss, R. F., Porter, L. W., Langenfelds, R. L., Wang, H. J., Emmons, L., Tie, X. X., and Dlugokencky, E. J.: In situ measurements of atmospheric methane at GAGE/AGAGE sites during 1985–2000 and resulting source inferences, J. Geophys. Res., 107, 4225, http://dx.doi.org/10.1029/2001JD001226doi:10.1029/2001JD001226, 2002.

De Mazière, M., Vigouroux, C., Bernath, P. F., Baron, P., Blumenstock, T., Boone, C., Brogniez, C., Catoire, V., Coffey, M., Duchatelet, P., Griffith, D., Hannigan, J., Kasai, Y., Kramer, I., Jones, N., Mahieu, E., Manney, G. L., Piccolo, C., Randall, C., Robert, C., Senten, C., Strong, K., Taylor, J., Tétard, C., Walker, K. A., and Wood, S.: Validation of ACE-FTS v2.2 methane profiles from the upper troposphere to the lower mesosphere, Atmos. Chem. Phys., 8, 2421–2435, http://dx.doi.org/10.5194/acp-8-2421-2008doi:10.5194/acp-8-2421-2008, 2008.

Denning, A. S., Holzer, M., Gurney, K. R., Heimann, M., Law, R. M., Rayner, P. J., Fung, I. Y., Fan, S., Taguchi, S., Friedlingstein, P., Balkanski, Y., Taylor, J., Maiss, M., and Levin, I.: Three-dimensional transport and concentration of SF_6: a model intercomparison study (TransCom-2), Tellus B, 51, 266–297, 1999.

Dentener, F., van Weele, M., Krol, M., Houweling, S., and van Velthoven, P.: Trends and inter-annual variability of methane emissions derived from 1979–1993 global CTM simulations, Atmos. Chem. Phys., 3, 73–88, http://dx.doi.org/10.5194/acp-3-73-2003doi:10.5194/acp-3-73-2003, 2003.

Dlugokencky, E. J., Masarie, K. A., Lang, P. M., and Tans, P. P.: Continuing decline in the growth rate of the atmospheric methane burden, Nature, 393(6684), 447–450, 1998.

Dlugokencky, E. J., Houweling, S., Bruhwiler, L., Masarie, K. A., Lang, P. M., Miller, J. B., and Tans, P. P.: Atmospheric methane levels off: temporary pause or a new steady-state?, Geophys. Res. Lett., 30(19), 1992, http://dx.doi.org/10.1029/2003GL018126doi:10.1029/2003GL018126, 2003.

Dlugokencky, E. J., Myers, R. C., Lang, P. M., Masarie, K. A., Crotwell, A. M., Thoning, K. W., Hall, B. D., Elkins, J. W., and Steele, L. P.: Conversion of NOAA atmospheric dry air CH_4 mole fractions to a gravimetrically prepared standard scale, J. Geophys. Res., 110, D18306, http://dx.doi.org/10.1029/2005JD006035doi:10.1029/2005JD006035, 2005.

Emmons, L. K., Walters, S., Hess, P. G., Lamarque, J.-F., Pfis-

ter, G. G., Fillmore, D., Granier, C., Guenther, A., Kinnison, D., Laepple, T., Orlando, J., Tie, X., Tyndall, G., Wiedinmyer, C., Baughcum, S. L., and Kloster, S.: Description and evaluation of the Model for Ozone and Related chemical Tracers, version 4 (MOZART-4), Geosci. Model Dev., 3, 43–67, http://dx.doi.org/10.5194/gmd-3-43-2010doi:10.5194/gmd-3-43-2010, 2010.

Etiope, G. and Milkov, A. V.: A new estimate of global methane flux from onshore and shallow submarine mud volcanoes to the atmosphere, Environ. Geol., 46, 997–1002, http://dx.doi.org/10.1007/s00254-004-1085-1doi:10.1007/s00254-004-1085-1, 2004.

Frankenberg, C., Warneke, T., Butz, A., Aben, I., Hase, F., Spietz, P., and Brown, L. R.: Pressure broadening in the $2\nu_3$ band of methane and its implication on atmospheric retrievals, Atmos. Chem. Phys., 8, 5061–5075, http://dx.doi.org/10.5194/acp-8-5061-2008doi:10.5194/acp-8-5061-2008, 2008.

Fraser, A., Chan Miller, C., Palmer, P. I., Deutscher, N. M., Jones, N. B., and Griffith, D. W. T.: The Australian methane budget: interpreting surface and train-borne measurements using a chemistry transport model, J. Geophys. Res., 116, D20306, doi:10.1029/2011JD015964, 2011.

Feng, W., Chipperfield, M. P., Dhomse, S., Monge-Sanz, B. M., Yang, X., Zhang, K., Ramonet, M., Evaluation of cloud convection and tracer transport in a three-dimensional chemical transport model, Atmos. Chem. Phys., 11, 5783-5803, doi:10.5194/acp-11-5783-2011, 2011.

Fung, I., John, J., Lerner, J., Matthews, E., Prather, M., Steele, L. P., and Fraser, P. J.: Three-dimensional model synthesis of the global methane cycle, J. Geophys. Res., 96(D7), 13033–13065, 1991.

Geller, L. S., Elkins, J. W., Lobert, J. M., Clarke, A. D., Hurst, D. F., Butler, J. H., and Myers, R. C.: Tropospheric SF_6: observed latitudinal distribution and trends, derived emissions and interhemispheric exchange time, Geophys. Res. Lett., 24, 675–678, 1997.

Gent, P. R., Yeager, S. G., Neale, R. B., Levis, S., and Bailey, D. A.: Improvements in a half degree atmosphere/land version of the CCSM, Clim. Dynam., 79, 25–58, http://dx.doi.org/10.1007/s00382-009-0614-8doi:10.1007/s00382-009-0614-8, 2009.

Gupta, M., Tyler, S., and Cicerone, R.: Modeling atmospheric $\delta^{13}CH_4$ and the causes of recent changes in atmospheric CH_4 amounts, J. Geophys. Res., 101(D17), 22923–22932, http://dx.doi.org/10.1029/96JD02386doi:10.1029/96JD02386, 1996.

Hein, R., Crutzen, P. J., and Heimann, M.: An inverse modeling approach to investigate the global atmospheric methane cycle, Global Biogeochem. Cy., 11, 43–76, 1997.

Hossaini, R., Chipperfield, M. P., Monge-Sanz, B. M., Richards, N. A. D., Atlas, E., and Blake, D. R.: Bromoform and dibromomethane in the tropics: a 3-D model study of chemistry and transport, Atmos. Chem. Phys., 10, 719–735, http://dx.doi.org/10.5194/acp-10-719-2010doi:10.5194/acp-10-719-2010, 2010.

Hourdin, F., Musat, I., Bony, S., Braconnot, P., Codron, F., Dufresne, J.-L., Fairhead, L., Filiberti, M.-A., Friedlingstein, P., Grandpeix, J.-Y., Krinner, G., Levan, P., and Lott, F.: The LMDZ4 general circulation model: climate performance and sensitivity to parametrized physics

with emphasis on tropical convection, Clim. Dynam., 27, 787–813, http://dx.doi.org/10.1007/s00382-006-0158-0doi:10.1007/s00382-006-0158-0, 2006.

Houweling, S., Kaminski, T., Dentener, F., Lelieveld, J., and Heimann, M.: Inverse modeling of methane sources and sinks using the adjoint of a global transport model, J. Geophys. Res., 104(D21), 26137–26160, 1999.

Houweling, S., Dentener, F., Lelieveld, J., Walter, B., and Dlugokencky, E.: The modeling of tropospheric methane: how well can point measurements be reproduced by a global model?, J. Geophys. Res., 105(D7), 8981–9002, 2000.

Huijnen, V., Williams, J., van Weele, M., van Noije, T., Krol, M., Dentener, F., Segers, A., Houweling, S., Peters, W., de Laat, J., Boersma, F., Bergamaschi, P., van Velthoven, P., Le Sager, P., Eskes, H., Alkemade, F., Scheele, R., Nédélec, P., and Pätz, H.-W.: The global chemistry transport model TM5: description and evaluation of the tropospheric chemistry version 3.0, Geosci. Model Dev., 3, 445–473, http://dx.doi.org/10.5194/gmd-3-445-2010doi:10.5194/gmd-3-445-2010, 2010.

Ito, A.: Changing ecophysiological processes and carbon budget in East Asian ecosystems under near-future changes in climate: implications for long-term monitoring from a process-based model, J. Plant Res., 123, 577–588, 2010.

Jacob, D. J., Prather, M. J., Rasch, P. J., Shia, R.-L., Balkanski, Y. J., Beagley, S. R., Bergmann, D. J., Blackshear, W. T., Brown, M., Chiba, M., Chipperfield, M. P., Grandpré, J. D., Dignon, J. E., Feichter, J., Genthon, C., Grose, W. L., Kashibhatla, P. S., Kohler, I., Kritz, M. A., Law, K., Penner, J. E., Ramonet, M., Reeves, C. E., Rotman, D. A., Stockwell, D. Z., Velthoven, P. F. J. V., Verver, G., Wild, O., Yang, H., and Zimmermann, P.: Evaluation and intercomparison of global atmospheric transport models using ^{222}Rn and other short-lived tracers, J. Geophys. Res., 102(D5), 5953–5970, 1997.

Kalnay, E., Kanamitsu, M., Kistler, R., Collins, W., Deaven, D., Gandin, L., Iredell, M., Saha, S., White, G., Woollen, J., Zhu, Y., Chelliah, M., Ebisuzaki, W., Higgins, W., Janowiak, J., Mo, K. C., Ropelewski, C., Wang, J., Leetmaa, A., Reynolds, R., Jenne, R., and Joseph, D.: The NCEP/NCAR 40-yr reanalysis project, B. Am. Meteorol. Soc., 77, 437–470, 1996.

Kanakidou, M., Dentener, F. J., Brasseur, G. P., Berntsen, T. K., Collins, W. J., Hauglustaine, D. A., Houweling, S., Isaksen, I. S. A., Krol, M., Lawrence, M. G., Muller, J. F. Poisson, N., Roelofs, G. J., Wang, Y., and Wauben, W. M. F.: 3-D global simulations of tropospheric CO distributions – results of the GIM/IGAC intercomparison 1997 exercise, Chemosph. Global Change Sci., 1, 263–282, 1999.

Kanamitsu, M., Ebisuzaki, W., Woollen, J., Yang, S. K., Hnilo, J. J., Fiorino, M., and Potter, G. L.:, NCEP-DOE AMIP-II reanalysis (R-2), B. Am. Meteorol. Soc., 83, 1631–1643, 2002.

Kawa, S. R., Erickson III, D. J., Pawson, S., and Zhu, Z.: Global CO_2 transport simulations using meteorological data from the NASA data assimilation system, J. Geophys. Res., 109, D18312, http://dx.doi.org/10.1029/2004JD004554doi:10.1029/2004JD004554, 2004.

Krol, M. C., van Leeuwen, P.-J., and Lelieveld, J.: Global OH trend inferred from methylchloroform measurements, J. Geophys. Res., 103, 10697–10711, 1998.

Krol, M. C., Lelieveld, J., Oram, D. E., Sturrock, G. A., Penkett, S. A., Brenninkmeijer, C. A. M., Gros, V., Williams, J.,

and Scheeren, H. A.: Continuing emissions of methyl chloroform from Europe, Nature, 421, 131–135, 2003.

Krol, M., Houweling, S., Bregman, B., van den Broek, M., Segers, A., van Velthoven, P., Peters, W., Dentener, F., and Bergamaschi, P.: The two-way nested global chemistry-transport zoom model TM5: algorithm and applications, Atmos. Chem. Phys., 5, 417–432, http://dx.doi.org/10.5194/acp-5-417-2005doi:10.5194/acp-5-417-2005, 2005.

Lamarque, J.-F., Bond, T. C., Eyring, V., Granier, C., Heil, A., Klimont, Z., Lee, D., Liousse, C., Mieville, A., Owen, B., Schultz, M. G., Shindell, D., Smith, S. J., Stehfest, E., Van Aardenne, J., Cooper, O. R., Kainuma, M., Mahowald, N., McConnell, J. R., Naik, V., Riahi, K., and van Vuuren, D. P.: Historical (1850–2000) gridded anthropogenic and biomass burning emissions of reactive gases and aerosols: methodology and application, Atmos. Chem. Phys., 10, 7017–7039, http://dx.doi.org/10.5194/acp-10-7017-2010doi:10.5194/acp-10-7017-2010, 2010.

Lambert, G. and Schmidt, S.: Reevaluation of the oceanic flux of methane: uncertainties and long term variations, Chemosph. Global Change Sci., 26, 579–589, 1993.

Langenfelds, R. L., Francey, R. J., Pak, B. C., Steele, L. P., Lloyd, J., Trudinger, C. M., and Allison, C. E.: Interannual growth rate variations of atmospheric CO$_2$ and its δ^{13}C, H$_2$, CH$_4$, and CO between 1992 and 1999 linked to biomass burning, Global Biogeochem. Cy., 16(3), 1048, 2002.

Law, R. M., Rayner, P. J., Denning, A. S., Erickson, D., Fung, I. Y., Heimann, M., Piper, S. C., Ramonet, M., Taguchi, S., Taylor, J. A., Trudinger, C. M., and Watterson, I. G.: Variations in modeled atmospheric transport of carbon dioxide and the consequences for CO$_2$ inversions, Global Biogeochem. Cy., 10, 783–796, http://dx.doi.org/10.1029/96GB01892doi:10.1029/96GB01892, 1996.

Law, R. M., Kowalczyk, E. A., and Wang, Y. P.: Using atmospheric CO$_2$ data to assess a simplified carbon-climate simulation for the 20th century, Tellus B, 53, 427–437, http://dx.doi.org/10.1111/j.1600-0889.2006.00198.xdoi:10.1111/j.1600-0889.2006.00198.x, 2006.

Law, R. M., Peters, W., Rodenbeck, C., Aulagnier, C., Baker, I., Bergmann, D. J., Bousquet, P., Brandt, J., Bruhwiler, L., Cameron-Smith, P. J., Christensen, J. H., Delage, F., Denning, A. S., Fan, S., Geels, C., Houweling, S., Imasu, R., Karstens, U., Kawa, S. R., Kleist, J., Krol, M. C., Lin, S.-J., Lokupitiya, R., Maki, T., Maksyutov, S., Niwa, Y., Onishi, R., Parazoo, N., Patra, P. K., Pieterse, G., Rivier, L., Satoh, M., Serrar, S., Taguchi, S., Takigawa, M., Vautard, R., Vermeulen, A. T., and Zhu, Z.: TransCom model simulations of hourly atmospheric CO$_2$: experimental overview and diurnal cycle results for 2002, Global Biogeochem. Cy., 22, GB3009, http://dx.doi.org/10.1029/2007GB003050doi:10.1029/2007GB003050, 2008.

Levin, I. and Hesshaimer, V.: Refining of atmospheric transport model entries by the globally observed passive tracer distributions of ^{85}krypton and sulfur hexafluoride (SF$_6$), J. Geophys. Res., 101, 16745–16755, 1996.

Levin, I., Naegler, T., Heinz, R., Osusko, D., Cuevas, E., Engel, A., Ilmberger, J., Langenfelds, R. L., Neininger, B.,

Rohden, C. v., Steele, L. P., Weller, R., Worthy, D. E., and Zimov, S. A.: The global SF$_6$ source inferred from long-term high precision atmospheric measurements and its comparison with emission inventories, Atmos. Chem. Phys., 10, 2655–2662, http://dx.doi.org/10.5194/acp-10-2655-2010doi:10.5194/acp-10-2655-2010, 2010.

Matthews, E. and Fung, I.: Methane emissions from natural wetlands: Global distribution, area, and ecology of sources, Global Biogeochem. Cy., 1, 61–86, http://dx.doi.org/10.1029/GB001i001p00061doi:10.1029/GB001i001p00061, 1987.

McCulloch, A. and Midgley, P. M.: The history of methyl chloroform emissions: 1951–2000, Atmos. Environ., 35, 5311–5319, 2001.

Mikaloff-Fletcher, S. E., Tans, P. P., Bruhwiler, L. M., Miller, J. B., and Heimann, M.: CH$_4$ sources estimated from atmospheric observations of CH$_4$ and its ^{13}C/^{12}C isotopic ratios: 2. Inverse modeling of CH$_4$ fluxes from geographical regions, Global Biogeochem. Cy., 18, GB4005, http://dx.doi.org/10.1029/2004GB002224doi:10.1029/2004GB002224, 2004.

Mitchell, T. D. and Jones, P. D.: An improved method of constructing a database of monthly climate observations and associated high-resolution grids, Int. J. Climatol., 25, 693–712, http://dx.doi.org/10.1002/joc.1181doi:10.1002/joc.1181, 2005.

Montzka, S. A., Krol, M., Dlugokencky, E., Hall, B., Jockel, P., and Lelieveld, J.: Small interannual variability of global atmospheric hydroxyl, Science, 331, 67-69, doi: 10.1126/science.1197640, 2011.

Olivier, J. G. J. and Berdowski, J. J. M.: Global emissions sources and sinks, in: The Climate System, edited by: Berdowski, J., Guicherit, R., and Heij, B. J., ISBN 9058092550, A. A. Balkema Publishers/Swets & Zeitlinger Pub., Lisse, The Netherlands, 33–78, 2001.

Onogi, K., Tsutsui, J., Koide, H., Sakamoto, M., Kobayashi, S., Hatsushika, H., Matsumoto, T., Yamazaki, N., Kamahori, H., Takahashi, K., Kadokura, S., Wada, K., Kato, K., Oyama, R., Ose, T., Mannoji, N., and Taira, R.: The JRA-25 reanalysis, J. Meteorol. Soc. Jpn., 85, 369–432, 2007.

Park, J. H., Russell, J. M., Gordley, L. L., Drayson, S. R., Benner, D. C., McInerney, J. M., Gunson, M. R., Toon, G. C., Sen, B., Blavier, J. F., Webster, C. R., Zipf, E. C., Erdman, P., Schmidt, U., and Schiller, C.: Validation of halogen occultation experiment CH$_4$ measurements from the UARS, J. Geophys. Res., 101, 10183–10203, 1996.

Patra, P. K., Law, R. M., Peters, W., Rodenbeck, C., Takigawa, M., Aulagnier, C., Baker, I., Bergmann, D. J., Bousquet, P., Brandt, J., Bruhwiler, L., Cameron-Smith, P. J., Christensen, J. H., Delage, F., Denning, A. S., Fan, S., Geels, C., Houweling, S., Imasu, R., Karstens, U., Kawa, S. R., Kleist, J., Krol, M. C., Lin, S.-J., Lokupitiya, R., Maki, T., Maksyutov, S., Niwa, Y., Onishi, R., Parazoo, N., Pieterse, G., Rivier, L., Satoh, M., Serrar, S., Taguchi, S., Vautard, R., Vermeulen, A. T., and Zhu, Z.: TransCom model simulations of hourly atmospheric CO$_2$: analysis of synoptic-scale variations for the period 2002–2003, Global Biogeochem. Cy., 22, GB4013, http://dx.doi.org/10.1029/2007GB003081doi:10.1029/2007GB003081, 2008.

Patra, P. K., Takigawa, M., Ishijima, K., Choi, B.-C., Cunnold, D.,

Dlugokencky, E. J., Fraser, P., Gomez-Pelaez, A. J., Goo, T.-Y., Kim, J.-S., Krummel, P., Langenfelds, R., Meinhardt, F., Mukai, H., O'Doherty, S., Prinn, R. G., Simmonds, P., Steele, P., Tohjima, Y., Tsuboi, K., Uhse, K., Weiss, R., Worthy, D., and Nakazawa, T.: Growth rate, seasonal, synoptic, diurnal variations and budget of methane in lower atmosphere, J. Meteorol. Soc. Jpn., 87(4), 635–663, 2009a.

Patra, P. K., Takigawa, M., Dutton, G. S., Uhse, K., Ishijima, K., Lintner, B. R., Miyazaki, K., and Elkins, J. W.: Transport mechanisms for synoptic, seasonal and interannual SF$_6$ variations and "age" of air in troposphere, Atmos. Chem. Phys., 9, 1209–1225, http://dx.doi.org/10.5194/acp-9-1209-2009doi:10.5194/acp-9-1209-2009, 2009b.

Patra, P. K., Houweling, S., Krol, M., Bousquet, P., Bruhwiler, L., and Jacob, D.: Protocol for TransCom CH$_4$ intercomparison, Version 7, http://www.jamstec.go.jp/frcgc/research/d4/prabir/papers/TC_CH4protocol_v7.pdf (last access: 26 April 2010), 2010.

Pickett-Heaps, C. A., Jacob, D. J., Wecht, K. J., Kort, E. A., Wofsy, S. C., Diskin, G. S., Worthy, D. E. J., Kaplan, J. O., Bey, I., and Drevet, J.: Magnitude and seasonality of wetland methane emissions from the Hudson Bay Lowlands (Canada), Atmos. Chem. Phys., 11, 3773–3779, http://dx.doi.org/10.5194/acp-11-3773-2011doi:10.5194/acp-11-3773-2011, 2011.

Plumb, R. A.: A "tropical pipe" model of stratospheric transport, J. Geophys. Res., 101, 3957–3972, http://dx.doi.org/10.1029/95JD03002doi:10.1029/95JD03002, 1996.

Press, W. H., Teukolsky, S. A, Vetterling, W. T, Flannery, B. P.: Numerical Recipes: The Art of Scientific Computing, Cambridge University Press., New York, ISBN 0521308119, 1986.

Prigent, C., Papa, F., Aires, F., Rossow, W. B., and Matthews, E.: Global inundation dynamics inferred from multiple satellite observations, 1993–2000, J. Geophys. Res., 112, D12107, http://dx.doi.org/10.1029/2006JD007847doi:10.1029/2006JD007847, 2007.

Prinn, R. G., Weiss, R., Fraser, P., Simmonds, P., Cunnold, D., Alyea, F., O'Doherty, S., Salameh, P., Miller, B., Huang, J., Wang, R., Hartley, D., Harth, C., Steele, L., Sturrock, G., Midgley, P., and McCulloch, A.: A history of chemically and radiatively important gases in air deduced from ALE/GAGE/AGAGE, J. Geophys. Res., 105, 17751–17792, http://dx.doi.org/10.1029/2000JD900141doi:10.1029/2000JD900141, 2000.

Prinn, R. G., Huang, J., Weiss, R. F., Cunnold, D. M., Fraser, P. J., Simmonds, P. G., McCulloch, A., Harth, C., Reimann, S., Salameh, P., O'Doherty, S., Wang, R. H. J., Porter, L. W., Miller, B. R., and Krummel, P. B.: Evidence for variability of atmospheric hydroxyl radicals over the past quarter century, Geophys. Res. Lett., 32, L07809, http://dx.doi.org/10.1029/2004GL022228doi:10.1029/2004GL022228, 2005.

Rasmussen, R. A. and Khalil, M. A. K.: Atmospheric methane in recent and ancient atmospheres: concentrations, trends, and interhemispheric gradient, J. Geophys. Res., 89, 11599–11605, 1984.

Rigby, M., Prinn, R. G., Fraser, P. J., Simmonds, P. G., Langenfelds, R. L., Huang, J., Cunnold, D. M., Steele, L. P., Krummel, P. B., Weiss, R. F., O'Doherty, S.,

Salameh, P. K., Wang, H. J., Harth, C. M., Muhle, J., and Porter, L. W.: Renewed growth of atmospheric methane, Geophys. Res. Lett., 35, L22805, http://dx.doi.org/10.1029/2008GL036037doi:10.1029/2008GL036037, 2008.

Rigby, M., Mühle, J., Miller, B. R., Prinn, R. G., Krummel, P. B., Steele, L. P., Fraser, P. J., Salameh, P. K., Harth, C. M., Weiss, R. F., Greally, B. R., O'Doherty, S., Simmonds, P. G., Vollmer, M. K., Reimann, S., Kim, J., Kim, K.-R., Wang, H. J., Olivier, J. G. J., Dlugokencky, E. J., Dutton, G. S., Hall, B. D., and Elkins, J. W.: History of atmospheric SF$_6$ from 1973 to 2008, Atmos. Chem. Phys., 10, 10305–10320, http://dx.doi.org/10.5194/acp-10-10305-2010doi:10.5194/acp-10-10305-2010, 2010.

Ringeval, B., de Noblet-Ducoudré, N., Ciais, P., Bousquet, P., Prigent, C., Papa, F., and Rossow, W. B.: An attempt to quantify the impact of changes in wetland extent on methane emissions on the seasonal and interannual time scales, Global Biogeochem. Cy., 24, GB2003, http://dx.doi.org/10.1029/2008GB003354doi:10.1029/2008GB003354, 2010.

Rotman, D. A., Atherton, C., Bergmann, D. J., Cameron-Smith, P. J., Chuang, C. C., Connell, P. S., Dignon, J. E., Franz, A., Grant, K. E., Kinnison, D. E., Molenkamp, C. R., Proctor, D. D., and Tannahill, J. R.: IMPACT, the LLNL 3-D global atmospheric chemical transport model for the combined troposphere and stratosphere: model description and analysis of ozone and other trace gases, J. Geophys. Res., 109, D04303, http://dx.doi.org/10.1029/2002JD003155doi:10.1029/2002JD003155, 2004.

Sander, S. P., Golden, D. M., Kurylo, M. J., Moortgat, G. K., Keller-Rudek, H., Wine, P. H., Ravishankara, A. R., Kolb, C. E., Molina, M. J., Finlayson-Pitts, B. J., Huie, R. E., and Orkin, V. L.: Chemical Kinetics and Photochemical Data for Use in Atmospheric Studies, Evaluation Number 15, JPL Publication 06-2, Jet Propulsion Laboratory, California Institute of Technology, Pasadena, CA, 2006.

Shindell, D. T., Faluvegi, G., Stevenson, D. S., Krol, M. C., Emmons, L. K., Lamarque, J.-F., Petron, G., Dentener, F. J., Ellingsen, K., Schultz, M. G., Wild, O., Amann, M., Atherton, C. S., Bergmann, D. J., Bey, I., Butler, T., Cofala, J., Collins, W. J., Derwent, R. G., Doherty, R. M., Drevet, J., Eskes, H. J., Fiore, A. M., Gauss, M., Hauglustaine, D. A., Horowitz, L. W., Isaksen, I. S. A., Lawrence, M. G., Montanaro, V., Muller, J. F., Pitari, G., Prather, M. J., Pyle, J. A., Rast, S., Rodriguez, J. M., Sanderson, M. G., Savage, N. H., Strahan, S. E., Sudo, K., Szopa, S., Unger, N., van Noije, T. P. C., and Zeng, G.: Multi-model simulations of carbon monoxide: comparison with observations and projected near-future changes, J. Geophys. Res., 111, D19306, http://dx.doi.org/10.1029/2006JD007100doi:10.1029/2006JD007100, 2006.

Shindell, D. T., Faluvegi, G., Koch, D. M., Schmidt, G. A., Unger, N., and Bauer, S. E.: Improved attribution of climate forcing to emissions, Science, 326, 716–718, http://dx.doi.org/10.1126/Science.1174760doi:10.1126/Science.1174760, 2009.

Simpson, I. J., Rowland, F. S., Meinardi, S., and Blake, D. R.: Influence of biomass burning during re-

cent fluctuations in the slow growth of global tropospheric methane, Geophys. Res. Lett., 33, L22808, http://dx.doi.org/10.1029/2006GL027330doi:10.1029/2006GL027330, 2006.

Spivakovsky, C., Logan, J. A., Montzka, S. A., Balkanski, Y. J., Foreman-Fowler, M., Jones, D. B. A., Horowitz, L. W., Fusco, A. C., Brenninkmeijer, C. A. M., Prather, M. J., Wofsy, S. C., McElroy, M. B.: Three-dimensional climatological distribution of tropospheric OH: update and evaluation, J. Geophys. Res., 105(D7), 8931–8980, 2000.

Stevenson, D. S., Dentener, F. J., Schultz, M. G., Ellingsen, K., van Noije, T. P. C., Wild, O., Zeng, G., Amann, M., Atherton, C. S., Bell, N., Bergmann, D. J., Bey, I., Butler, T., Cofala, J., Collins, W. J., Derwent, R. G., Doherty, R. M., Drevet, J., Eskes, H. J., Fiore, A. M., Gauss, M., Hauglustaine, D. A., Horowitz, L. W., Isaksen, I. S. A., Krol, M. C., Lamarque, J.-F., Lawrence, M. G., Montanaro, V., Muller, J.-F., Pitari, G., Prather, M. J., Pyle, J. A., Rast, S., Rodriguez, J. M., Sanderson, M. G., Savage, N. H., Shindell, D. T., Strahan, S. E., Sudo, K., and Szopa, S.: Multimodel ensemble simulations of present-day and near-future tropospheric ozone, J. Geophys. Res., 111, D08301, http://dx.doi.org/10.1029/2005JD006338doi:10.1029/2005JD006338, 2006.

Sudo, K., Takahashi, M., Kurokawa, J., and Akimoto, H.: CHASER: a global chemical model of the troposphere 1. Model description, J. Geophys. Res., 107, 4339, http://dx.doi.org/10.1029/2001JD001113doi:10.1029/2001JD001113, 2002.

Takigawa, M., Takahashi, M., and Akiyoshi, H.: Simulation of ozone and other chemical species using a Center for Climate System Research/National Institute for Environmental Studies atmospheric GCM with coupled stratospheric chemistry, J. Geophys. Res., 104, 14003–14018, 1999.

Uppala, S. M., Koallberg, P. W., Simmons, A. J., Andrae, U., da Costa Bechtold, V., Fiorino, M., Gibson, J. K., Haseler, J., Hernandez, A., Kelly, G., Li, X., Onogi, K., Saarinen, S., Sokka, N., Allan, R. P., Andersson, E., Arpe, K., Balmaseda, M. A., Beljaars, A. C. M., van de Berg, L., Bidlot, J., Bormann, N., Caires, S., Chevallier, F., Dethof, A., Dragosavac, M., Fisher, M., Fuentes, M., Hagemann, S., Holm, E., Hoskins, B. J., Isaksen, L., Janssen, P. A. E. M., Jenne, R., McNally, A. P. A., Mahfouf, J.-F., Morcrette, J.-J., Rayner, N. A., Saunders, R. W., Simon, P., Sterl, A., Trenberth, K. E., Untch, A., Vasiljevic, D., Viterbo, P., and Woollen, J.: The ERA-40 re-analysis, Q. J. Roy. Meteorol. Soc., 131, 2961–3012, http://dx.doi.org/10.1256/qj.04.176doi:10.1256/qj.04.176, 2005.

van der Werf, G. R., Randerson, J. T., Giglio, L., Collatz, G. J., Kasibhatla, P. S., and Arellano Jr., A. F.: Interannual variability in global biomass burning emissions from 1997 to 2004, Atmos. Chem. Phys., 6, 3423–3441, http://dx.doi.org/10.5194/acp-6-3423-2006doi:10.5194/acp-6-3423-2006, 2006.

Velders, G.: Description of the RIVM 2-dimensional stratosphere model, RIVM Report 722201002, The Netherland, 1995.

Wang, J. S., Logan, J. A., McElroy, M. B., Duncan, B. N., Megretskaia, I. A., and Yantosca, R. M.: A 3-D model analysis of the slowdown and interannual variability in the methane growth rate from 1988 to 1997, Global Biogeochem. Cy., 18, GB3011, http://dx.doi.org/10.1029/2003GB002180doi:10.1029/2003GB002180,

2004.

WDCGG – WMO World Data Centre for Greenhouse Gases: Japan Meteorological Agency, Tokyo, online available at: http://gaw.kishou.go.jp/wdcgg.html (last access: 19 April 2010), 2010.

WMO/SAOD, World Meteorological Organization, Scientific Assessment of Ozone Depletion: Global Ozone Research Monitoring Project – Report No. 47, WMO, Geneva, 498 pp., 2003.

Wofsy, S. C., the HIPPO Science Team and Cooperating Modellers and Satellite Teams: HIAPER pole-to-pole observations (HIPPO): fine grained, global scale measurements for determining rates for transport, surface emissions, and removal of climatologically important atmospheric gases and aerosols, Philos. T. Roy. Soc. A, 369, 2073–2086, 2011.

Xiong, X., Barnet, C. D., Maddy, E., Sweeney, C., Liu, X., Zhou, L., and Goldberg, M.: Characterization and validation of methane products from the atmospheric infrared sounder (AIRS), J. Geophys. Res., 113, G00A01, http://dx.doi.org/10.1029/2007JG000500doi:10.1029/2007JG000500, 2008.

Yan, X., Akiyama, H., Yagi, K., and Akimoto, H.: Global estimations of the inventory and mitigation potential of methane emissions from rice cultivation conducted using the 2006 intergovernmental panel on climate change guidelines, Global Biogeochem. Cy., 23, GB2002, http://dx.doi.org/10.1029/2008GB003299doi:10.1029/2008GB003299, 2009.

Yoshida, Y., Ota, Y., Eguchi, N., Kikuchi, N., Nobuta, K., Tran, H., Morino, I., and Yokota, T.: Retrieval algorithm for CO_2 and CH_4 column abundances from short-wavelength infrared spectral observations by the Greenhouse gases observing satellite, Atmos. Meas. Tech., 4, 717–734, http://dx.doi.org/10.5194/amt-4-717-2011doi:10.5194/amt-4-717-2011, 2011.

Table 1. List of tracers simulated in the TransCom-CH_4 intercomparison project. See Sect. 2.2 for a description of the CH_4 flux components; e.g., cyclostationary natural (CYC NAT), interannually varying anthropogenic (IAV ANT), biomass burning (BB), wetland (WL).

PARAMETERS	DESCRIPTION	TIME RESOLUTION
CH_4 tracers using different emission secnarios		
1. CH_4_CTL	CYC NAT (CYC BB & CYC WL) + IAV ANT EDGAR 3.2	Monthly; Partial IAV
2. CH_4_CTL_E4	CYC NAT + IAV ANT EDGAR4.0	Monthly; Partial IAV
3. CH_4_BB	CYC NAT − 0.35 CYC BB + IAV BB + IAV ANT EDGAR 3.2	Monthly; Partial IAV
4. CH_4_WL_BB	CYC NAT − 0.35 CYC BB + IAV BB − CYC WL + 0.76 IAV WL + IAV ANT EDGAR 3.2	Monthly; Full IAV
5. CH_4_INV	IPSL/LSCE inversion	Monthly; Full IAV
6. CH_4_EXTRA*	CYC NAT − 0.35 CYC BB + IAV BB − CYC WL − Rice + IAV WLe (0.69 Wetland + 0.895 Rice) + IAV ANT EDGAR 3.2	Monthly; Full IAV
Other species/tracers		
7. SF_6	EDGAR4.0; Global totals modified	Annual; Full IAV
8. Radon-222 (^{222}Rn)	1.0 and 0.1 atom m^{-2} s^{-1} over land and ocean, respectively	Annual; No IAV
9. CH_3CCl_3 (MCF)	EDGAR3.2 with trends and distributions modified	Annual; Full IAV

* this scenario is called EXTRA because the VISIT terrestrial ecosystem model (Ito, 2010) fluxes are still under evaluation, but included here since no other bottom-up wetland emission scenario was available with IAV for the full simulation period at the time the intercomparison protocol was released. VISIT is driven by climate variables from the Climate Research Unit time series version 3.0 (CRU TS3.0) dataset (Mitchell and Jones, 2005; updated values) and NCEP/NCAR reanalysis (Kalnay et al., 1996) for the periods of 1988–2005 and 2006–2007, respectively, and CH_4 cycling in the inundated areas is modeled using the scheme of Cao et al. (1998 and references therein).

Table 2. Overview of participating transport models and model variants, and average lifetimes of atmospheric CH_4 and CH_3CCl_3 are given.

Sl. No.	Model Name[a]	Institution[b]	Resolution Horizontal[c]	Vertical[d]	Meteorology[e]	Avg. lifetime (1992–07)[f] CH_4_CTL	CH_3CCl_3
1	**ACCESS**	CSIRO	$3.75 \times 2.5°$	38	AGCM; SST	9.93 ± 0.13	4.55 ± 0.15
2	**ACTM**	RIGC	$\sim 2.8 \times 2.8°$	67σ	NCEP2; U, V, T; SST	10.0 ± 0.10	4.60 ± 0.13
2a	*ACTM_OH*[$]	RIGC	$\sim 2.8 \times 2.8°$	67σ	NCEP2; U, V, T; SST	9.51 ± 0.10	4.84 ± 0.13
3	CAM	CU	$2.5 \times \sim 1.9°$	28σ	NCEP/NCAR	10.2 ± 0.11	3.77 ± 0.13
4	**CCAM**	CSIRO	~ 220 km	18σ	NCEP; U, V; SST	9.94 ± 0.27	4.01 ± 0.15
5	GEOS-Chem	UoE	$2.5 \times 2.0°$	$30/47\eta$	NASA/GSFC/GEOS4/5	9.60 ± 0.11	4.70 ± 0.13
5a	*GEOS-Chem_DOH*	UoE	$2.5 \times 2.0°$	$30/47\eta$	NASA/GSFC/GEOS4/5	9.95 ± 0.11	4.84 ± 0.13
6	IMPACT	LLNL	$5.0 \times 4.0°$	55η	NASA/GSFC/GEOS4	10.1 ± 0.05	4.63 ± 0.3
6a	*IMPACT_1 $\times$ 1.25*	LLNL	$1.25 \times 1.0°$	55η	NASA/GSFC/GEOS4	9.99 ± 0.07	4.54 ± 0.16
7	**LMDZ**	LSCE	$3.75 \times 2.5°$	19η	ECMWF; U, V, T; SST	10.0 ± 0.09	3.90 ± 0.25
8	MOZART	MIT	$\sim 1.8 \times 1.8°$	28σ	NCEP/NCAR	9.88 ± 0.15	3.90 ± 0.15
9	NIES08i	NIES	$2.5 \times 2.5°$	32σ-θ	JCDAS, ERA-interim-PBL	10.0 ± 0.06	4.75 ± 0.02
10	PCTM	GSFC	$1.25 \times 1.0°$	58η	NASA/GSFC/GEOS5	10.1 ± 0.1	4.54 ± 0.21
11	TM5	SRON	$6.0 \times 4.0°$	25η	ECMWF, ERA-interim	10.1 ± 0.12	4.87 ± 0.03
11a	*TM$_5$_1 $\times$ 1*	SRON	$1.0 \times 1.0°$	25η	ECMWF, ERA-interim	10.1 ± 0.11	4.88 ± 0.14
12	TOMCAT	UoL	$\sim 2.8 \times 2.8°$	60η	ECMWF, ERA-40/interim	9.98 ± 0.12	4.71 ± 0.18

[a] CTMs driven by AGCM transport are identified in bold (nudging parameters in right-most column), and model variants are shown in italics. The model variants are indicated by post-fixed parameters, following a "_".

[b] CSIRO: Commonwealth Scientific and Industrial Research Organisation, Australia; GSFC: NASA Goddard Space Flight Center, USA; RIGC: Research Institute for Global Change, Japan; CU: Cornel University, USA; LLNL: Lawrence Livermore National Laboratory, USA; LSCE: Laboratoire des Sciences du Climat et de l'Environnement, France; NIES: National Institute for Environmental Studies, Japan; SRON: Netherlands Institute for Space Research; UoE: University of Edinburgh, UK; UoL: University of Leeds, UK.

[c] Longitude $\times$ latitude or distance or spectral resolution indicated by T (triangular) maximum wave number (T42 and T63 for $\sim 2.8 \times 2.8°$ and $\sim 1.8 \times 1.8°$, respectively).

[d] Terrain-following (height) coordinate system for ACCESS, σ vertical coordinates are pressure divided by surface pressure, η vertical coordinates are a hybrid sigma-pressure coordinate (GEOS-Chem has 30 or 47 layers for 1990–2006 or 2007, respectively), NIES08i has a hybrid sigma-isentropic.

[e] The source of meteorology (NCEP2 (AMIP DOE II): Kanamitsu et al., 2002; NCEP: Kalnay et al., 1996; NASA/GSFC/GEOS4/5: Bloom et al., 2005; ECMWF: Uppala et al., 2005; JCDAS: Onogi et al., 2007) and parameters used in nudged AGCMs are given.

[f] The averaging period for IMPACT_1 $\times$ 1.25 (2002-2007) and TM5_1 $\times$ 1 (2003-2007) differ.

[$] The tropospheric OH field is taken from CHASER full chemistry model [Sudo et al., 2002] and scaled by $\times 0.88$, and stratospheric OH is taken from AGCM (Takigawa et al., 1999) as discussed in Patra et al. (2009a). SF_6 emissions are used from EDGAR4.0 without scaling the global totals to match with Levin et al. (2010).

Table 3. Multi-model averages ($\pm 1\sigma$; and between model variability defined by 1σ/average, within parenthesis in %) of simulated SF_6 (ppt), CH_4_CTL (ppb), CH_3CCl_3 (ppt) and ^{222}Rn ($\times 10^{-21}$) gradients in the troposphere and UT/LS region for three broad latitude bands, namely, the SH midlatitude, tropics and NH midlatitude.

Species	SH (60–30° S)	Tropics (15° S–15° N)	NH (30–60° N)
Tropospheric gradients			
Difference between:	850–400 mb	850–200 mb	850–400 mb
SF_6	-0.026 ± 0.005 (18 %)	0.044 ± 0.017 (39 %)	0.128 ± 0.018 (14 %)
CH_4	-9.91 ± 2.57 (26 %)	17.18 ± 7.69 (45 %)	44.65 ± 5.91 (13 %)
CH_3CCl_3	0.473 ± 0.145 (31 %)	0.295 ± 0.182 (62 %)	1.01 ± 0.25 (25 %)
^{222}Rn	0.984 ± 0.527 (54 %)	8.66 ± 2.73 (32 %)	23.90 ± 6.73 (28 %)
UT/LS gradients			
Difference between:	200–100 mb	100–50 mb	200–100 mb
SF_6	0.158 ± 0.074 (47 %)	0.264 ± 0.148 (56 %)	0.229 ± 0140 (61 %)
CH_4	84.45 ± 35.89 (43 %)	124.04 ± 65.07 (52 %)	128.77 ± 64.96 (50 %)
CH_3CCl_3	7.86 ± 1.37 (17 %)	16.59 ± 4.48 (27 %)	9.79 ± 3.75 (38 %)
^{222}Rn	1.084 ± 0.708 (65 %)	0.415 ± 0.203 (49 %)	0.353 ± 0445 (126 %)

Table 4. Average (across all models) correlation coefficient (r) between model simulated and observed seasonal cycles and interannual variation of CH$_4$, SF$_6$ and CH$_3$CCl$_3$.

Tracer \ Site*	ALT	BRW	MHD	MLO	RPB	SMO	CGO	SPO
			For seasonal cycles (2002–2003)					
CH$_4$_CTL	**.16 ± .3**	**-.09 ± .2**	.73 ± .1	.63 ± .1	.86 ± .1	.74 ± .2	.98 ± .02	.96 ± .1
CH$_4$_CTL_E4	**.21 ± .3**	**-.10 ± .3**	.72 ± .1	.69 ± .1	.88 ± .1	.71 ± .2	.97 ± .02	.96 ± .1
CH$_4$_BB	**.10 ± .3**	**-.11 ± .2**	.68 ± .1	.66 ± .1	.86 ± .1	.72 ± .2	.95 ± .1	.96 ± .1
CH$_4$_WL_BB	**.38 ± .3**	.48 ± .2	.42 ± .2	.70 ± .1	.86 ± .1	.64 ± .3	.94 ± .1	.95 ± .1
CH$_4$_INV	.88 ± .1	.63 ± .2	.92 ± .1	.74 ± .1	.88 ± .1	.61 ± .2	.95 ± .02	.92 ± .1
CH$_4$_EXTRA	.84 ± .1	**.37 ± .2**	.79 ± .1	.50 ± .2	.80 ± .1	.69 ± .3	.93 ± .1	.95 ± .1
SF$_6$	.48 ± .2	**.23 ± .2**	.68 ± .1	**-.06 ± .1**	**.13 ± .2**	.70 ± .4	.43 ± .2	.50 ± .2
CH$_3$CCl$_3$	.78 ± .1	.93 ± .02	.87 ± .1	.91 ± .1	.96 ± .02	.89 ± .1	.88 ± .1	.81 ± 1
			For interannual variations (CH$_4$, CH$_3$CCl$_3$: 1991–2007; SF$_6$: 1996–2007)					
CH4_CTL	.52 ± .2	.14 ± .2	.66 ± .1	.32 ± .2	.34 ± .2	.38 ± .2	.46 ± .2	.43 ± .2
CH4_CTL_E4	.27 ± .2	.01 ± .2	.46 ± .2	-.02 ± .2	.05 ± .3	.24 ± .2	.03 ± .2	-.06 ± .2
CH$_4$_BB	.69 ± .2	.40 ± .2	.76 ± .1	.47 ± .2	.75 ± .1	.54 ± .2	.60 ± .2	.57 ± .2
CH$_4$_WL_BB	.55 ± .2	.47 ± .2	.51 ± .2	.38 ± .2	.68 ± .2	.53 ± .2	.48 ± .1	.46 ± .2
CH$_4$_INV	.64 ± .1	.32 ± .2	.68 ± .1	.27 ± .2	.42 ± .2	.38 ± .2	.63 ± .2	.56 ± .2
CH$_4$_EXTRA	.61 ± .2	.36 ± .2	.77 ± .1	.51 ± .2	.77 ± .2	.73 ± .1	.68 ± .1	.69 ± .1
SF$_6$	.33 ± .2	.67 ± .1	.75 ± .2	.70 ± .2	–	.34 ± .1	.83 ± .1	.81 ± .1
CH$_3$CCl$_3$	.97 ± .03	.97 ± .03	.95 ± .04	.96 ± .03	.95 ± .04	.96 ± .04	.95 ± .03	.94 ± .03

* ALT (Alert, Canada; 62° W, 82° N, 210 m), BRW (Point Barrow, Alaska, USA; 157° W, 71° N, 11 m), MLO (Mauna Loa Observatory, Hawaii, USA; 156° W, 20° N, 3397 m) and SPO (South Pole Observatory, Antarctica; 25° W, 90° S, 2810 m) are managed under the NOAA cooperative network by the Global Monitoring Division, Earth System Research Laboratory (GMD/ESRL) (Dlugokencky et al., 1998; Butler et al., 2004), and MHD (Mace Head, Ireland; 10° W, 53° N, 25 m), RPB (Ragged Point, Barbados; 59° W, 13° N, 45 m), SMO (Samoa, USA; 171° W, 14° S, 42 m) and CGO (Cape Grim, Australia; 145° E, 41° S, 94 m) sites are operated under the AGAGE network by the Massachusetts Institute of Technology (MIT, USA), Scripps Institutions of Oceanography, University of California, San Diego (SIO/UCSD, USA), Commonwealth Scientific and Industrial Research Organization (CSIRO, Australia), University of Bristol, UK and Georgia Institute of Technology, USA (Cunnold et al., 2002; Prinn et al., 2000)
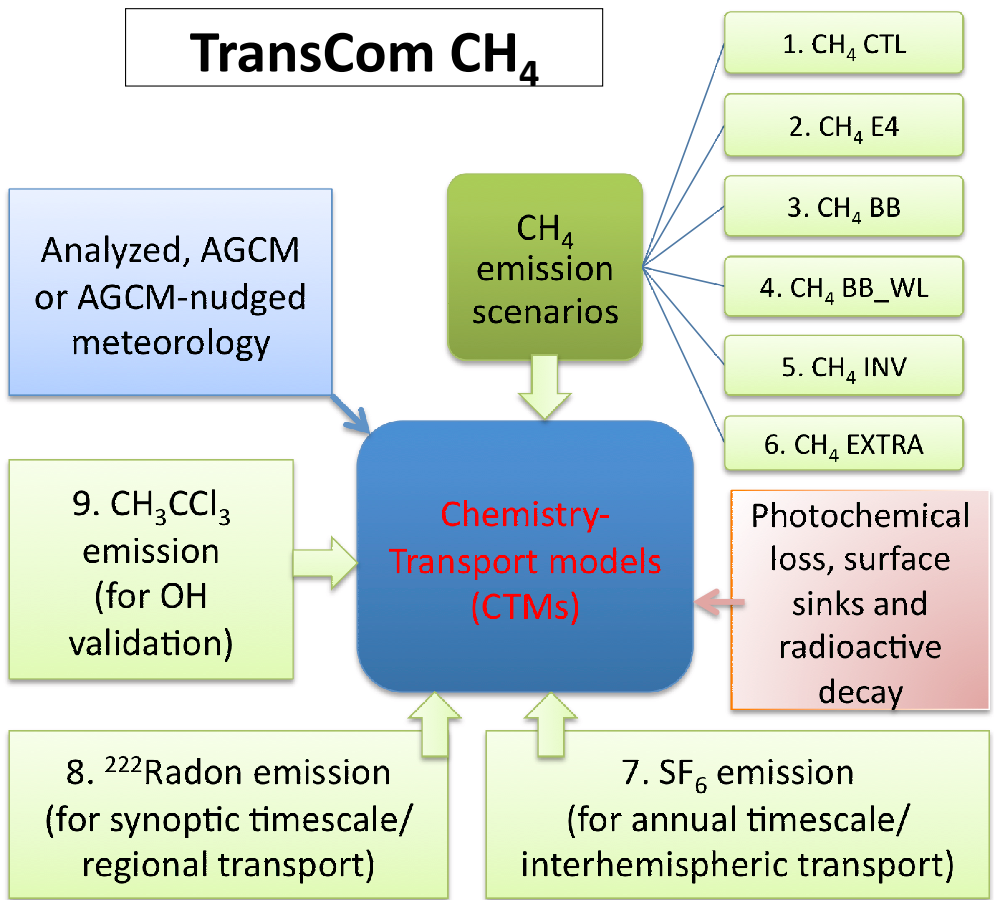
Fig. 1. Schematic diagram of TransCom-CH$_4$ model simulation experiment.
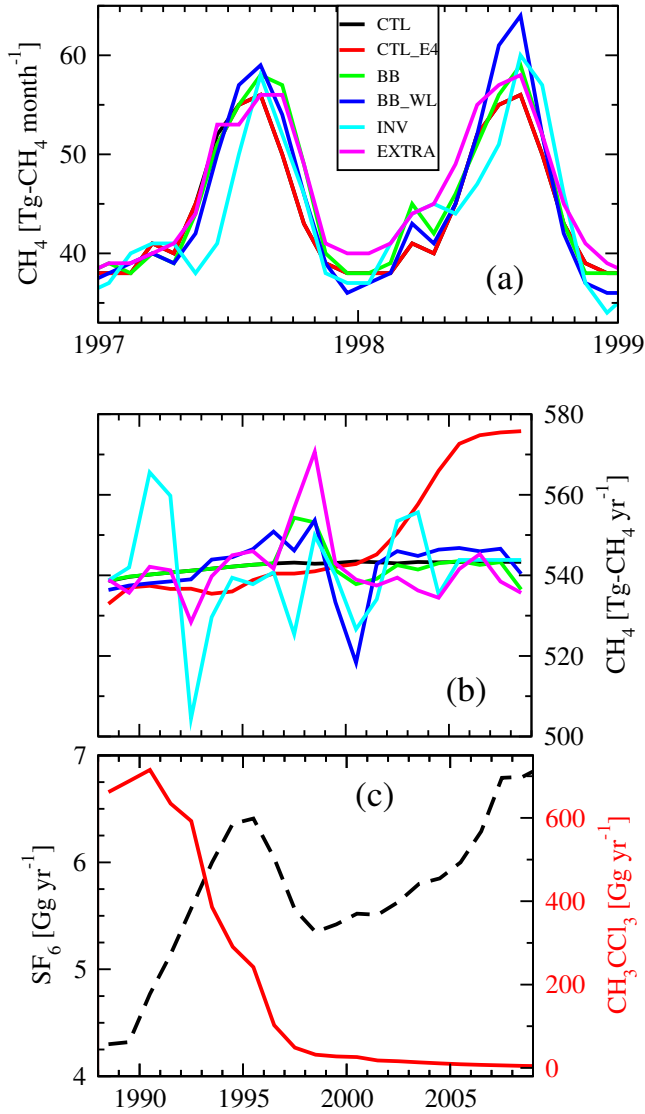
Fig. 2. Examples of CH_4 emission seasonalities corresponding to the years 1997 and 1998 are shown in **(a)** (the black line is hidden behind the red line), and annual mean CH_4 emissions for the period of 1988–2008 are depicted in **(b)**. The annual mean SF_6 and CH_3CCl_3 fluxes are shown in **(c)**.
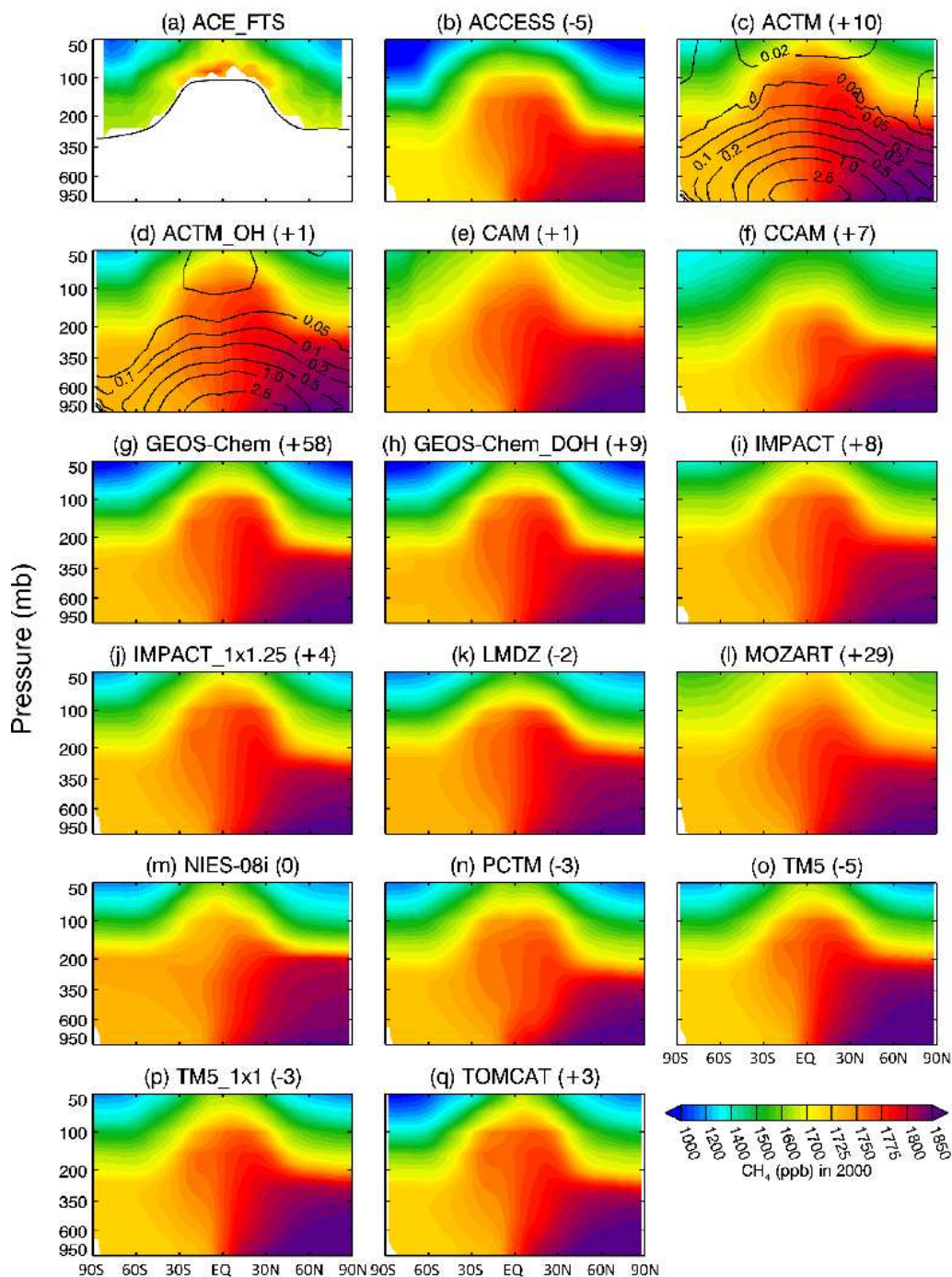
Fig. 3. Annual and zonal mean latitude-pressure (in mb) cross-sections of CH$_4$ for tropospheric and lower stratospheric altitudes as observed by the ACE-FTS instrument (**a**; climatology) and as simulated by the models in 2000 (**b–o**). The black line in (**a**) shows the climatological tropopause height. The contour lines in (**c** and **d**) show CH$_4$ loss rate (units: molecule cm^{-3} s^{-1}) as in the ACTM and ACTM_OH, respectively. An offset is added to the concentrations in each panel (given after the model name in ppb) that adjusts the model fields to a common average value of 1770 ppb between 950 mb and 500 mb. Detailed model-to-model comparisons for ^{222}Rn, SF$_6$, CH$_4$ and CH$_3$CCl$_3$ for two seasons and over two longitudes are available in the Supplement (Figs. S1–S17).
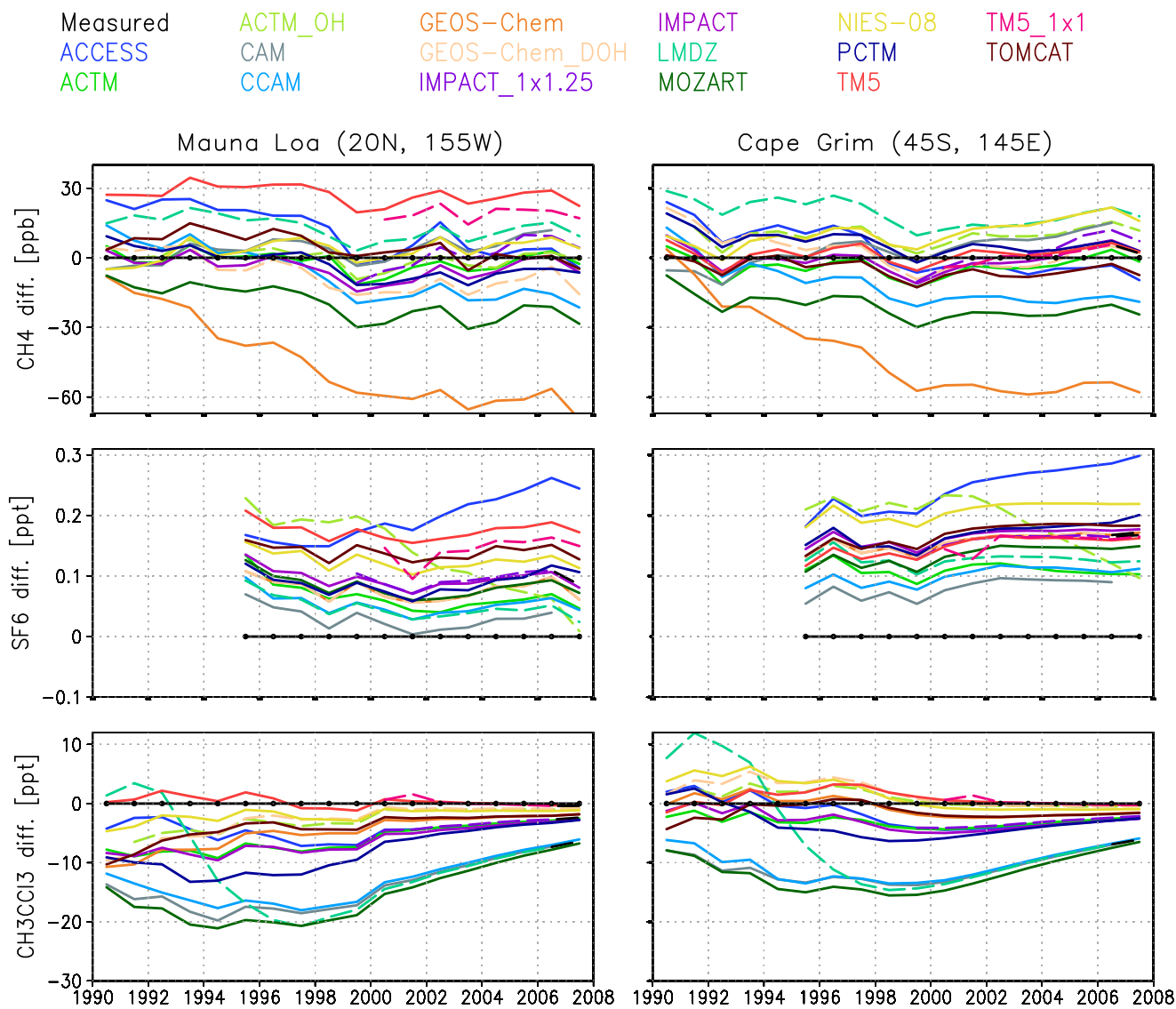
Fig. 4. Time series of differences between observed and simulated annual mean CH$_4$ in CH$_4$_CTL scenario (top row), SF$_6$ (middle row) and CH$_3$CCl$_3$ (bottom row) at two selected sites: MLO (left column) and CGO (right column). Time series of annual mean values and tropospheric model values, averaged over 1000–200 mb and all latitudes/longitudes, are shown in Figs. S18 and S19, respectively.
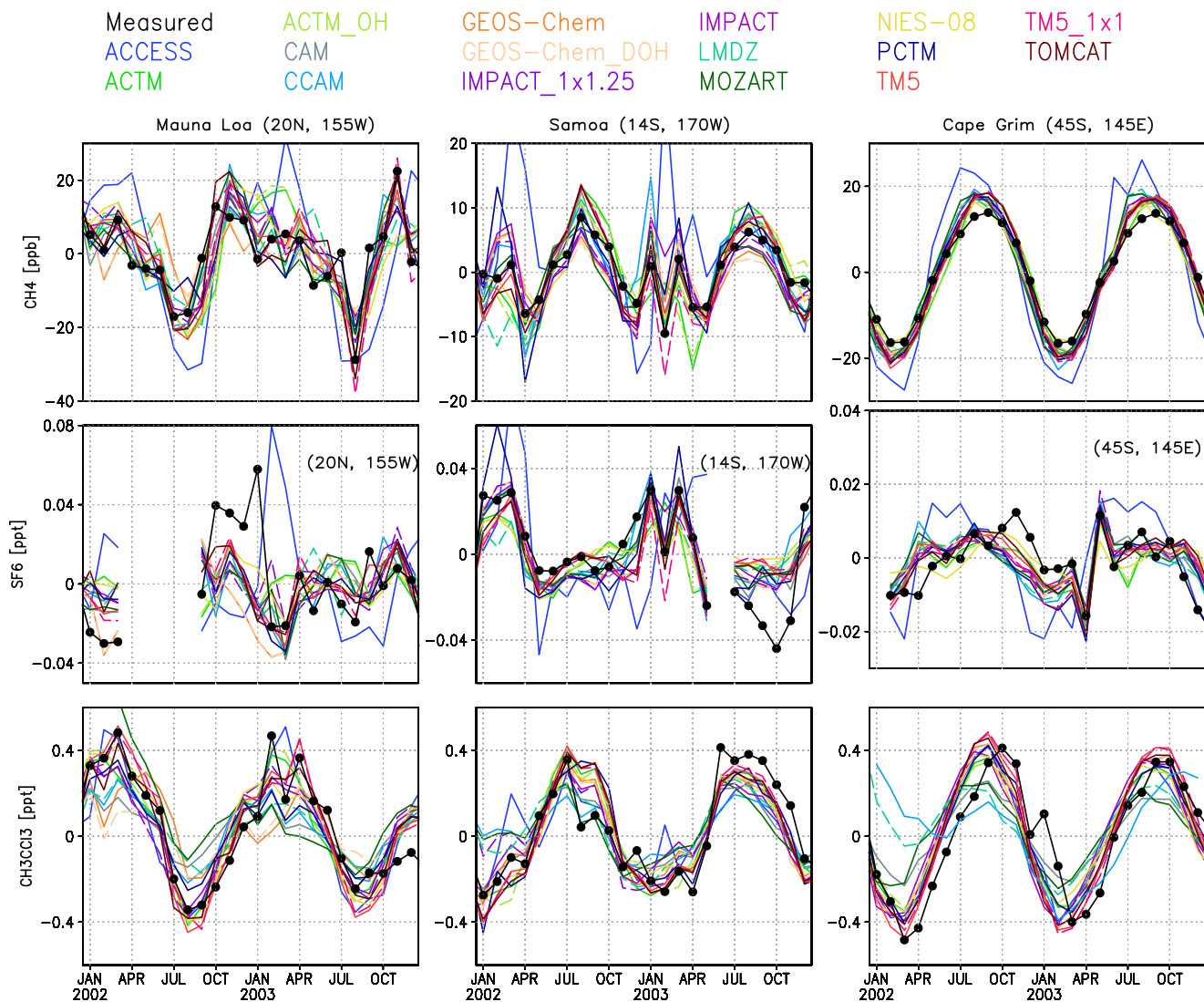
Fig. 5. Comparisons of observed and simulated seasonal cycles of CH$_4$ in CH$_4$_CTL scenario (top row), SF$_6$ (middle row) and CH$_3$CCl$_3$ (bottom row) at 3 selected sites, MLO (left panel), SMO (middle panel) and CGO (right panel).
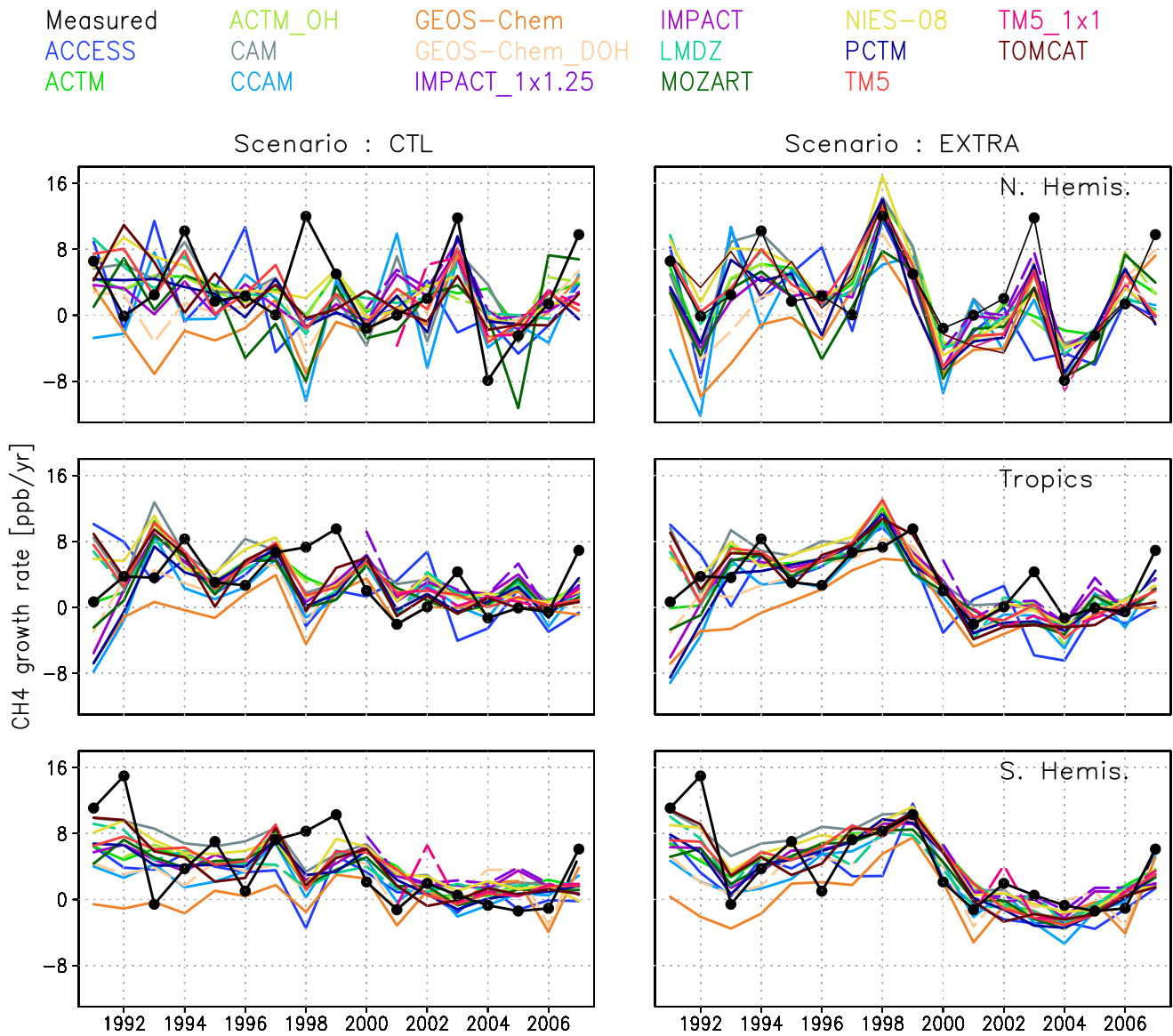
Fig. 6. Comparisons of observed and simulated annual mean growth rates of CH_4 in NH (top row; ALT, BRW and MHD average), tropics (middle row; MLO RPB and SMO average) and SH (bottom row; CGO and SPO average) for two selected fluxes, CTL (left column) and EXTRA (right column). Growth rate variabilities corresponding 4 other CH_4 scenarios are given in Figs. S20 and S21.
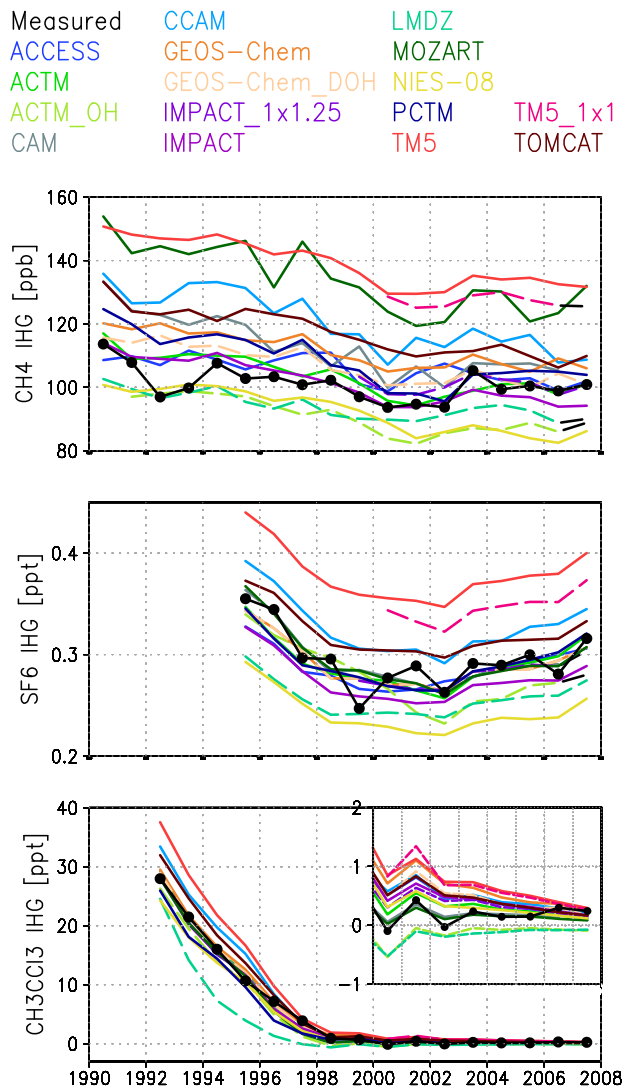
Fig. 7. Interhemispheric gradients (IHGs) for CH$_{4\_C}TL$, SF_6 and CH$_3$CCl$_3$ concentrations between the NH (BRW, MLO) and SH (CGO, SPO) sites. The values at CGO (AGAGE) are adjusted to NOAA scales by adding an offset of 0.02 ppt for SF$_6$, and multiplied by 1.0003 and 1.0333 for CH$_4$ and MCF, respectively (see text in Sect. 2.4 for further details). Please note that adjustment of the AGAGE data to NOAA scale is made just for convenience. These 4 sites are chosen here because their data coverage is most complete during 1990–2007. Haley Bay (75.58° S, 26.5° W, 10 m) site is chosen for PCTM due to no SPO data in all files. Inset shows expanded y-axis view of MCF for the 2000–2007 period.
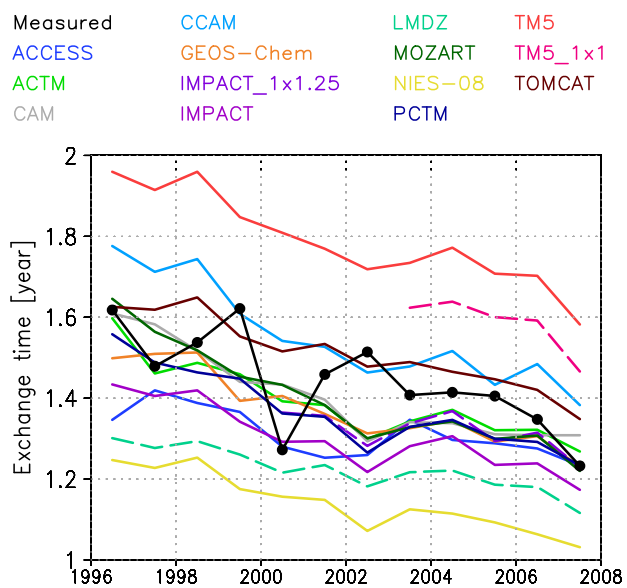
Fig. 8. IH exchange time (τ_{ex}) estimated using the measured and simulated time series of average SF$_6$ in NH (BRW, MLO) and SH (CGO, SPO) by employing Eqn. (4).
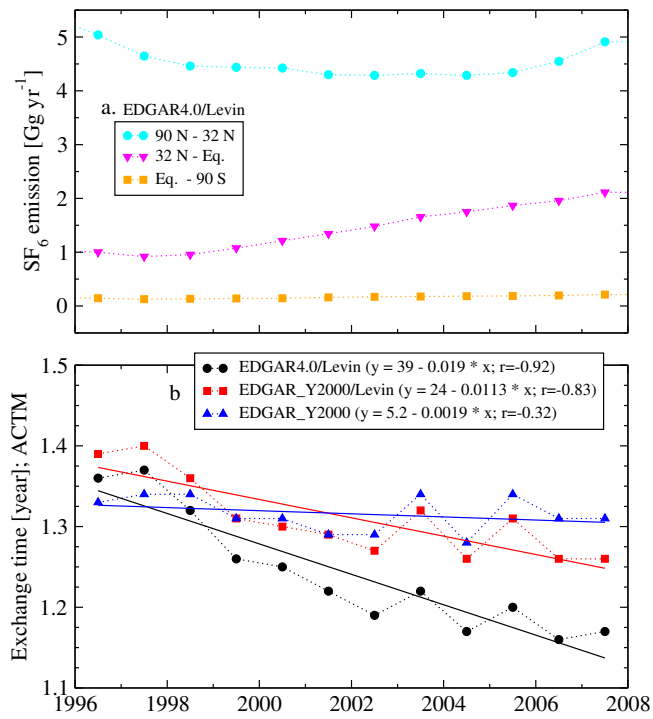
Fig. 9. SF$_6$ emissions in three broad latitude bands (a, top panel), and τ_{ex} (b, bottom panel) estimated using ACTM simulated SF$_6$ time series for three different emission scenarios.
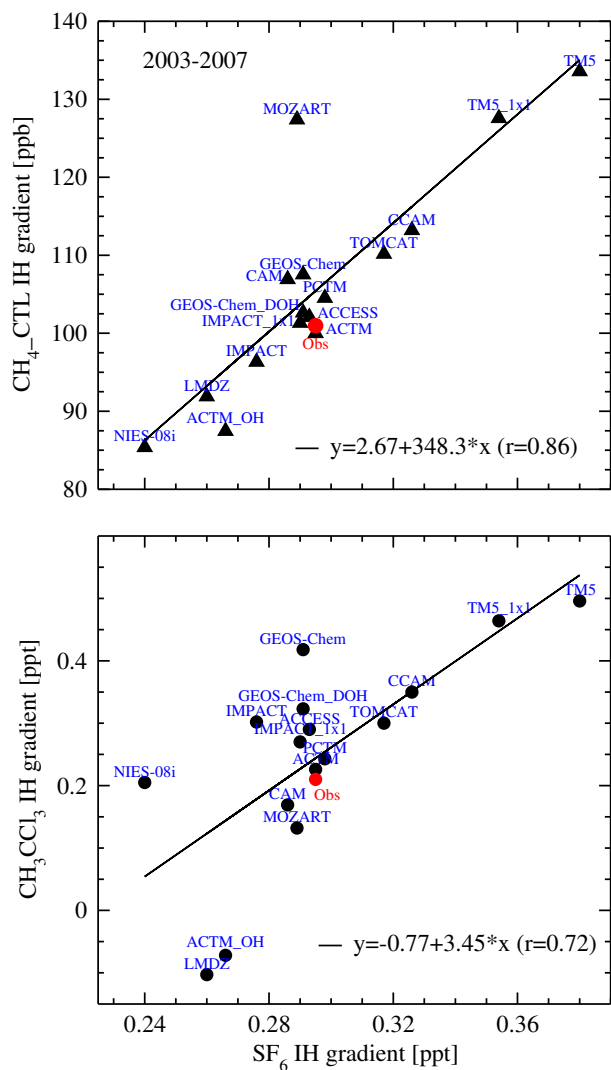
Fig. 10. Correlation between IH gradients of SF$_6$ with that of CH$_4$ and CH$_3$CCl$_3$ are depicted, using average values for the period 2003–2007 and for 4 sites as in Fig. 7. ACTM_OH is excluded here because the SF$_6$ emissions are not as per the protocol.
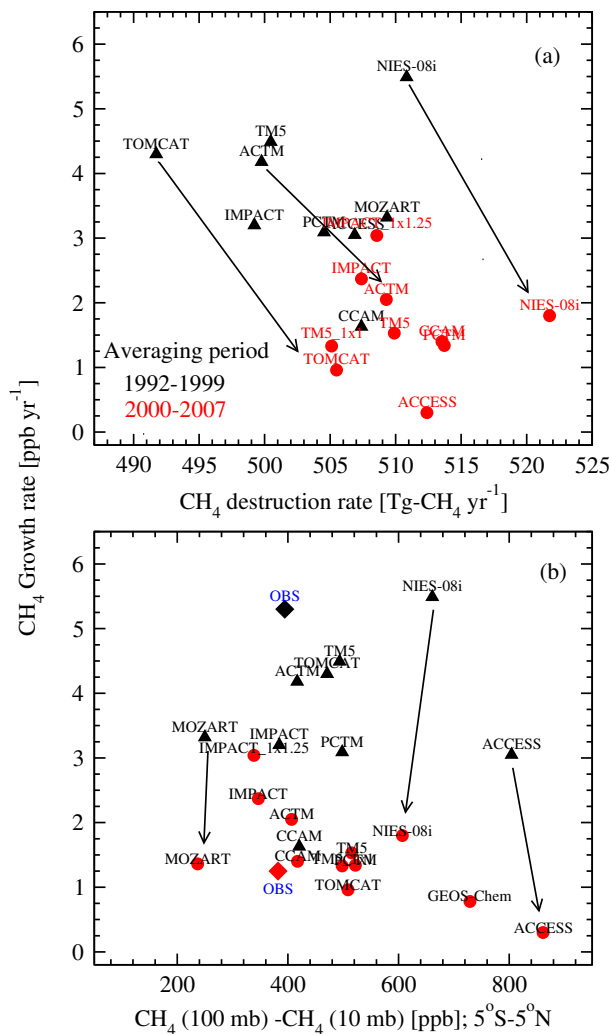
Fig. 11. Relationships of global loss rates for different models (CH$_4$_EXTRA) with their simulated growth rates at surface sites **(a)**, and the modeled vertical gradients in the lower stratosphere (100–10 mb layer; **b**) with growth rate. ACTM_OH and GEOS-Chem_DOH are excluded from this analysis as those models used different OH fields.
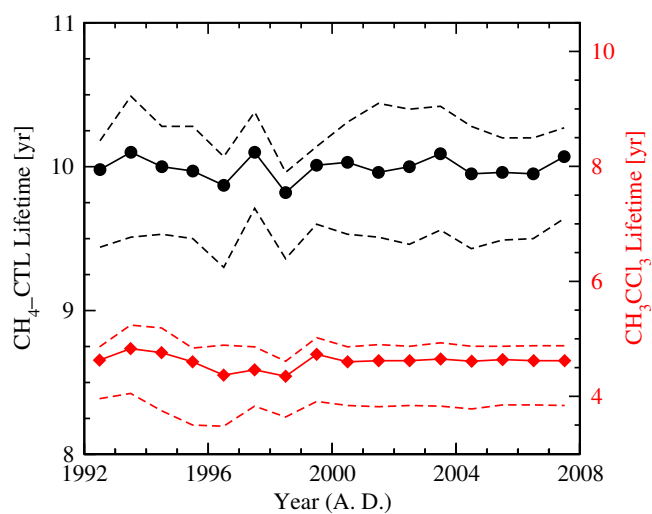
Fig. 12. Time series of median (symbols) and ranges (broken lines) of atmospheric lifetimes of CH$_4$ (black) and CH$_3$CCl$_3$ (red). Note that the mean CH$_4$ lifetimes for EXTRA (9.96 $\pm$ 0.08 yr) and CTL (9.99 $\pm$ 0.08 yr) fluxes agree within their interannual variability. A comparison of CH$_3$CCl$_3$ lifetimes calculated using Eqn. (5) and gridded photochemical destruction rates is shown in Fig. S22 (ACTM only).